Syntectonic emplacement of the Middle Jurassic Concón Mafic Dike Swarm, Coastal Range, central Chile (33° S)

Christian Creixell [a,*], Miguel Ángel Parada [a], Pierrick Roperch [b,c], Diego Morata [a], César Arriagada [a], Carlos Pérez de Arce [d]

[a] *Universidad de Chile, Departamento de Geología, Plaza Ercilla 803, casilla 13518, Santiago, Chile*
[b] *Universidad de Chile, Departamento de Geología, Institut de Recherche pour le Développement (IRD), Santiago, Chile*
[c] *IRD, UR154-LMTG and Géosciences Rennes, Campus de Beaulieu, 35042 Rennes cedex, France*
[d] *Servicio Nacional de Geología y Minería, Laboratorio de Geocronología, Tiltil 1998, Santiago, Chile*

Abstract

The Concón Mafic Dike Swarm (CMDS) consists of basaltic to andesitic dikes emplaced into deformed Late Paleozoic granitoids during the development of the Jurassic arc of central Chile. The dikes are divided into an early group of thick dikes (5–12 m) and a late group of thin dikes (0.5–3 m). Two new amphibole $^{40}Ar/^{39}Ar$ dates obtained from undeformed and deformed dikes, constrain the age of emplacement and deformation of the CMDS between 163 and 157 Ma. Based on radiometric ages, field observations, AMS studies and petrographic data, we conclude that the emplacement of the CMDS was syntectonic with the Jurassic arc extension and associated with sinistral displacements along the NW-trending structures that host the CMDS. The common occurrence of already deformed and rotated xenoliths in the dikes indicates that deformation in the granitoids started previously.

The early thick dikes and country rocks appear to have been remagnetized during the exhumation of deep-seated coastal rocks in the Early Cretaceous (around 100 Ma). The remanent magnetization in late thin dikes is mainly retained by small amounts of low-Ti magnetite at high temperature and pyrrhotite at low temperature. The magnetization in these dikes appears to be primary in origin. Paleomagnetic results from the thin dikes also indicate that the whole area was tilted ~23° to the NNW during cooling of the CMDS.

The NNW–SSE extension vectors deduced from the paleomagnetic data and internal fabric of dikes are different with respect to extension direction deduced for the Middle–Late Jurassic of northern Chile, pointing to major heterogeneities along the margin of the overriding plate during the Mesozoic or differences in the mechanisms driving extension during such period.

Keywords: Dike swarm; Magnetic fabric; Syntectonic emplacement; Middle Jurassic; Central Chile; Paleomagnetism; Block tilting

1. Introduction

Dike swarms are probably the main conduits for transport of magma from deep sources (upper mantle or lower crust) to the upper crust (e.g. Ernst et al., 2001). Dikes are magma-filled fractures originated or activated in association with extensional stresses. These structures can be found in various tectonic environments, such as passive volcanic margins (e.g. Callot and Geoffroy, 2004) or active continental margins (e.g. Glazner et al., 1999). Dikes can provide information about the composition of

* Corresponding author. Tel.: +56 2 9780642; fax: +56 2 6963050.
E-mail address: ccreixel@ing.uchile.cl (C. Creixell).

magma sources (e.g. Scarrow et al., 1998) and, because flow directions can be measured, the location of the magma reservoirs (e.g. Callot and Geoffroy, 2004). Paleostress trajectories can be inferred because these structures record the strain that occurs during their intrusion into the upper crust (Glazner et al., 1999; Mège and Korme, 2004). The strain can be recorded as relative displacements of structural markers or as occurrence of tensile fractures generated by the magmatic pressure (Delaney et al., 1986).

The classical interpretation of dike emplacement is that they form perpendicular to the minimum principal stress direction (e.g. Anderson, 1951). However, the internal structure of tabular magmatic bodies shows that, in some cases, fabrics develop in response to complex patterns of dilation associated with both internal (magmatic) and external (tectonic) stresses, and so they can form in directions not perpendicular to the minimum principal stress direction, especially when there are preexisting fractures. For example, oblique fabrics can be developed in dikes emplaced along shear structures, indicating an oblique pattern of aperture (e.g. Hutton, 1992; Glazner et al., 1999; Correa-Gomes et al., 2001).

Over the last fifteen years, there has been an increase in our knowledge of the internal architecture of tabular magmatic bodies such as dikes, mainly because AMS (Anisotropy of Magnetic Susceptibility) can be used to decipher the internal arrangement of magmatic rocks, even those with very low anisotropy (<3%). The preferred orientation of magnetic grains defines an ellipsoid with three main axis ($K_1 > K_2 > K_3$), where K_1 and K_3 represent the magnetic lineation and the pole of magnetic foliation, respectively. Sources for AMS come mainly from ferromagnetic grains and to a lesser degree from paramagnetic ferrosilicates. Several studies have shown that a good correspondence exists between the magnetic subfabric measured by AMS and the magmatic petrofabric of the rocks (Geoffroy et al., 2002; Ferré et al., 2003, and references therein). This is true because in most cases, magnetic grains (e.g. titanomagnetite) are later phases in the crystallization sequence, and tend to occupy spaces left by previously crystallized minerals. In most of these cases, the shape anisotropy (elongation of individual magnetic grains) is controlled by the texture of the rock, which is primarily defined by the alignment of individual mineral grains.

Mesozoic mafic dike swarms in the Coastal Range of central Chile have been described (e.g., Muñoz Cristi, 1964; Levi, 1973; Irwin et al., 1987; Parada et al., 1991), but the geological processes associated with their origin and evolution are still poorly understood. In central and north-central Chile, extensional tectonics during the Jurassic–Early Cretaceous have been inferred from geochemical and isotopic data (Vergara et al., 1995; Parada et al., 1999; Morata and Aguirre, 2003) and from stratigraphic relationships (Vergara et al., 1995), but an understanding of the underlying tectonic mechanisms remains illusive. Mafic dike swarms in this area provide an opportunity to increase our understanding of the plate kinematics and the timing of extension during development of the Middle Jurassic magmatic arc. These processes can be related directly to the mechanisms of magma transport and emplacement in the upper crust of this part of the central Andes.

In this paper we provide field, petrographic, AMS fabric and geochronological evidence for the emplacement of the Middle Jurassic Concón Mafic Dike Swarm (CMDS), one of the most important exposures of Mesozoic dike swarms in the Coastal Range of central Chile.

To better define the 3-D internal architecture of the fabric of the dikes and country rocks, we collected samples for AMS analysis along the entire width of the intrusions, and measured structural data in the field. The first objective of the AMS sampling was to obtain magma flow directions, but after the first field observations and AMS results, we reorganized the sampling procedure to focus on the deformational mechanisms. Field data were supplemented with geothermometric calculations in hornblende–plagioclase pairs and geochronology to broadly constrain the timing and nature of the fabric's development and to connect the fabric with possible emplacement mechanisms. Because effects of magmatic and tectonic stress could be present at high temperature during fabric acquisition, $^{40}Ar/^{39}Ar$ geochronology in hornblende appears to be the most feasible method to get an age closer to the real crystallization age. New paleomagnetic results of the same rocks were obtained, with the aim of better understanding the tectonic processes associated with Mesozoic extensional tectonics in the area. The emplacement of the CMDS is discussed in terms of the tectonic evolution of the Mesozoic arc magmatism of central Chile.

2. Geological setting

The Coastal Range of central Chile at ~33° S is composed of three plutonic belts and Mesozoic volcanic and sedimentary rocks that decrease in age to the east (Vergara et al., 1995; Parada et al., 1999; Fig. 1a). Late Paleozoic granitoids form the western belt; Mid-Jurassic intrusions occupy the central belt and Early Cretaceous plutonic rocks occupy the eastern belt. The Mesozoic volcanic and sedimentary formations were deposited in subsiding basins during the Early Jurassic–Early Cretaceous extensional regime (Vergara et al., 1995; Aguirre

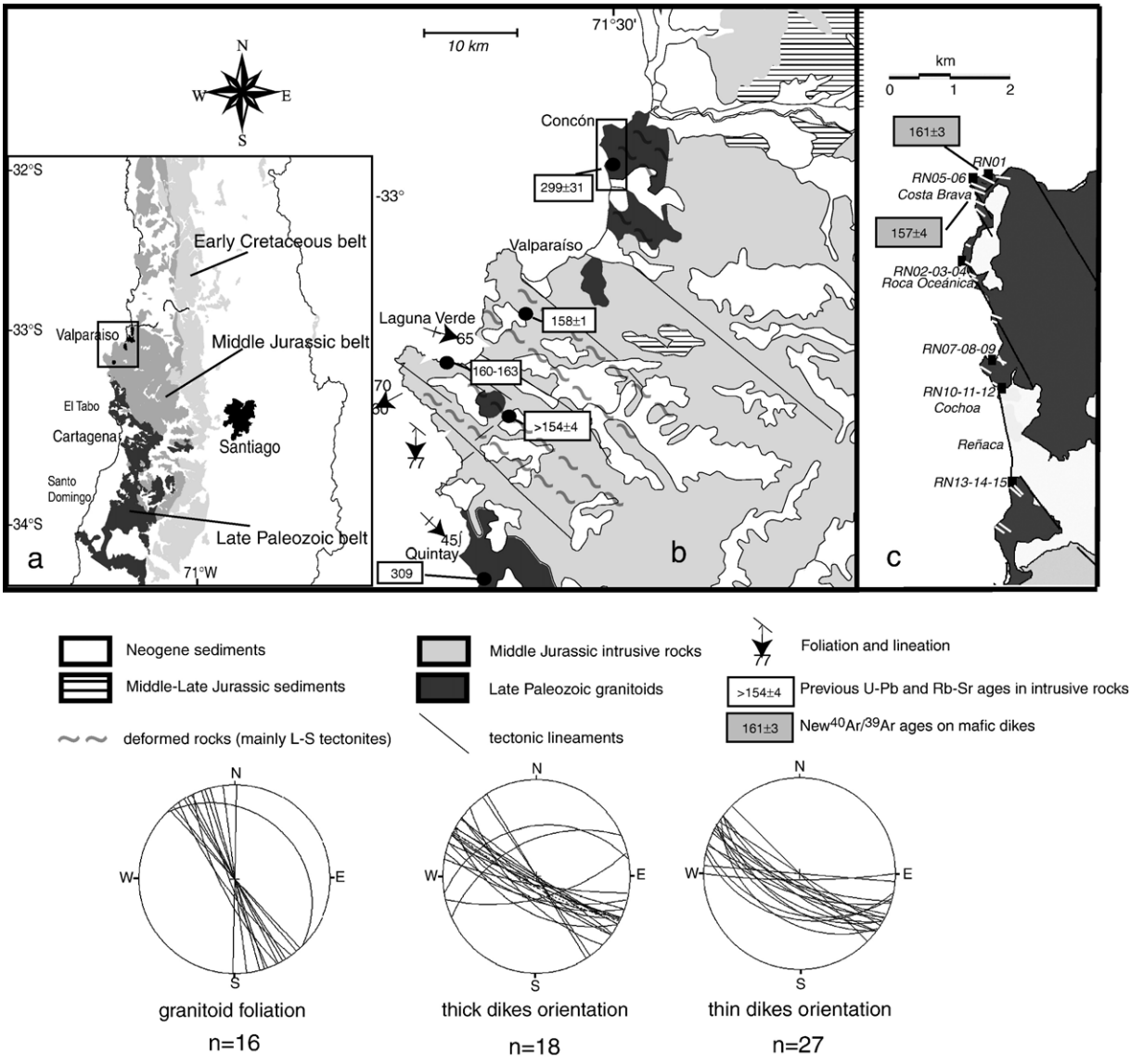

Fig. 1. (a) Simplified magmatic units in the Coastal Range of central Chile (modified from Parada et al., 1999) (b) Geological map of the Coastal Range near 33°, modified from Godoy and Loske (1988). Previous U–Pb ages are shown in squares. The exception is an age of 299±31 Ma from Rb–Sr isochron in granitoids from Reñaca. Inset figure at right (c) is a geological sketch of the study area, with location of sampling stations. White lines represent main dike exposures and black lines are main lineaments.

et al., 1999). A whole-rock Rb–Sr errorchron of 299± 31 Ma has been obtained (Hervé et al., 1988) for Late Paleozoic granitoids hosting the CMDS. This age does not differ from Rb–Sr and U–Pb ages of 290–309 Ma obtained elsewhere along the Late Paleozoic western belt between 33°10′ and 33°40′ S (Hervé et al., 1988; Godoy and Loske, 1988; Gana and Tosdal, 1996; see Table 1). The spatially restricted Late Triassic intrusive rocks close to the Late Paleozoic granitoids at Cartagena yielded a plutonic age of 214±1 Ma (U–Pb zircon, Gana and Tosdal, 1996). A similar age K–Ar age of 213±10 Ma was obtained by Cordani et al. (1976) for the same rocks (Table 1). The age of the Middle Jurassic granitoids of the central belt, which represent the plutonism suspected to be coeval with the CMDS, is well constrained by zircon and titanite U–Pb ages of 160–163 Ma (Godoy and Loske, 1988) from foliated diorites at Laguna Verde (33°10′ S, Fig. 1b). Part of these rocks were intruded along NW–SE structures, as suggested by Godoy and Loske (1988), based on field and geochronological data. Slightly

Table 1
Compilation of the main radiometric ages obtained in Paleozoic and Mesozoic plutonic and metamorphic rocks of the area, between 33° and 33°45′ S

Method	Material	Locality	Age (Ma) and error (2σ)	Author
Late Paleozoic granitoids				
Rb–Sr isochron	Whole rock	Santo Domingo	308±15	Hervé et al. (1988)
Rb–Sr isochron	Whole rock	Algarrobo	292±2	Hervé et al. (1988)
U–Pb	Zircon	Quintay	290	Godoy and Loske (1988)
U–Pb	Zircon	Quintay	309	Godoy and Loske (1988)
Rb–Sr errorchron	Whole rock	Reñaca	299±31	Hervé et al. (1988)
Fission track	Apatite	Algarrobo	98±10	Gana and Zentilli (2000)
Gneissic diorites and granitic gneisses				
U–Pb	Zircon	Cartagena	214±1	Gana and Tosdal (1996)
K–Ar	Amphibole	Cartagena	213±10	Cordani et al. (1976)
K–Ar	Amphibole	Cartagena	167+8	Cordani et al. (1976)
K–Ar	Plagioclase	Cartagena	157±1	Cordani et al. (1976)
K–Ar	Biotite	Cartagena	159±15	Hervé et al. (1988)
Rb–Sr	Whole rock	Las Cruces	162+48	Hervé et al. (1988)
Fission track	Apatite	Cartagena	106±8.6	Gana and Zentilli (2000)
Fission track	Apatite	Cartagena	106±7.4	Gana and Zentilli (2000)
Laguna Verde diorites and amphibolites				
U–Pb	Zircon	Laguna Verde	160–163	Godoy and Loske (1988)
Ar–Ar	Amphibole	Laguna Verde	165±2.6	Irwin et al. (1987)
Rb–Sr errorchron	Bt, feld, apatite, wr	Laguna Verde	156.3±1.2	Godoy and Loske (1988)
Jurassic granitoids				
U–Pb	Titanite	S of Valparaíso	157	Gana and Tosdal (1996)
U–Pb	Zircon	S of Valparaíso	>154+4	Gana and Tosdal (1996)
U–Pb	Zircon	S of Valparaíso	158±1	Gana and Tosdal (1996)
U–Pb	Titanite	Cantera Las Placillas	155.5	Gana and Tosdal (1996)
Rb–Sr errorchron	Whole rock	Cuesta Zapata	173±28	Hervé et al. (1988)
Mafic dikes				
Ar–Ar	Amphibole	Laguna Verde	169.6±3.6	Irwin et al.(1987)
K–Ar	Amphibole	Cartagena	133.1+7.2	Irwin et al. (1987)
Ar–Ar	Amphibole	El Tabo	172.4+2.4	Irwin et al. (1987)
K–Ar	Biotite	El Tabo	183.4+6	Irwin et al. (1987)
K–Ar	Plagioclase	El Tabo	179.4+4.8	Irwin et al. (1987)

younger U–Pb ages were reported by Gana and Tosdal (1996) in granitoids located directly to the east of Laguna Verde (Sauce Unit, Table 1). The age of the Early Cretaceous eastern plutonic belt of the Coastal Range, is constrained by a zircon U–Pb age in the interval 94.2–97.3 Ma, and several ^{40}Ar–^{39}Ar ages between 94.9±1.8 and 93.2± 1.1 Ma obtained for amphibole, biotite and plagioclase of the Caleu pluton (33° S, Parada et al., 2005). Biotite K–Ar ages in other Early Cretaceous plutons of the area range from 118 to 91 Ma (Corvalán and Munizaga, 1972; Gana et al., 1996).

The Mesozoic evolution (Jurassic–Early Cretaceous) of the Andean arc was characterized by the development of an extensional arc setting (Mpodozis and Ramos, 1989; Vergara et al., 1995; Parada et al., 1999) wherein marine sediments were deposited and mantle-derived magmas with progressively depleted isotopic signature were emplaced (Vergara et al., 1995; Parada et al., 1999; Morata et al., 2001). This tectonic scenario differs from the Paleozoic and Tertiary to recent Andean evolution which is characterized by compressive deformation and crustal thickening (Isacks, 1988; Parada et al., 1999). During the Mesozoic extensional period, abundant mafic dike swarms were emplaced, mostly intruding Paleozoic and Jurassic intrusions (Irwin et al., 1987, 1988), which appears to have been an important mechanism for magma transport.

3. Middle Jurassic deformation

In the Coastal Range between 33° and 33°45′ S (Fig. 1b), we have recognized a pervasive subvertical gneissic fabric in Late Paleozoic granitoids, mainly as L–

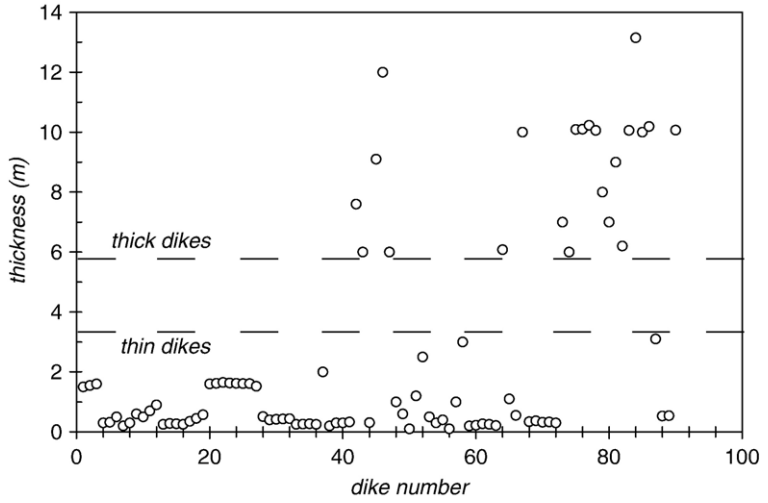

Fig. 2. Thickness (in meters) of dikes vs. number of measured dikes. A break in thickness between thick and thin dikes is observed between approximately 3 and 6 m.

S tectonites. In addition to this deformation, which probably occurred at high temperature during Late Paleozoic times, garnet-bearing gneissic granitoids at Cartagena, with a mylonitic fabric have been described (Gana et al., 1996), with normal dip-slip kinematics associated with a southdipping E–W foliation. Geochronological data suggest that this fabric originated during the Middle Jurassic (Hervé et al., 1988). These rocks are also intruded by Middle Jurassic dikes.

Structural and geochronological data in Middle Jurassic diorites in the Laguna Verde area indicate that these intrusions were syntectonically emplaced along NW structures (Irwin et al., 1987; Godoy and Loske, 1988). These rocks are characterized by a pervasive NW–WNW foliation (280–317°/71–87° S) and locally N–S (4–21°/42–72° S) with steeply dipping SSW to SSE-plunging stretching lineations, both defined by alignment of medium-grained feldspars and mafic minerals. Some of

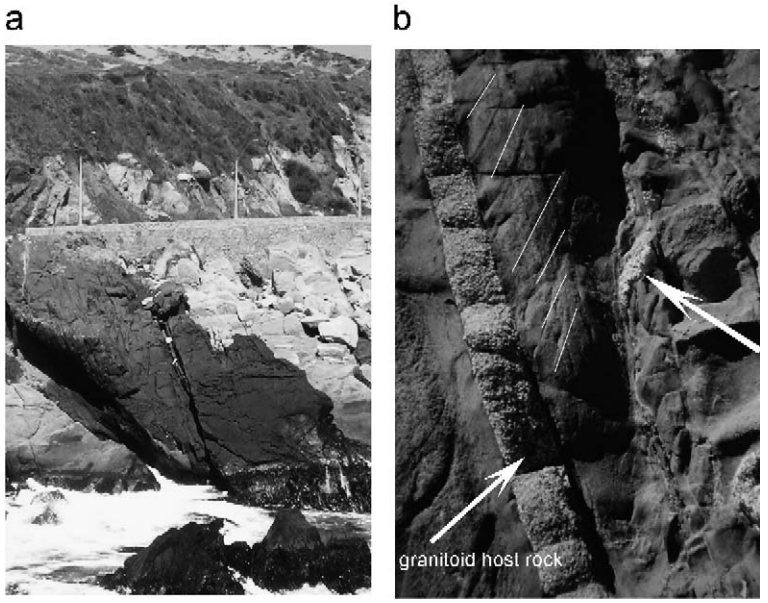

Fig. 3. Field features of dikes: a) thick dike (10 m thickness) tilted to the NNW at Roca Oceánica (see Fig. 1c for location). View to the east b) sinistral fabrics in vertical view of a thin dike (1.7 m thick), arrow indicates presence of sigmoidal granitoid xenolith, view from NW.

these foliated rocks show evidence of sub-vertical normal shearing. Geochronological data, coupled with geological and petrographical observations, suggest that the deformation occurred soon after emplacement.

4. Analythical methods

Microprobe analysis of mafic silicates (amphibole and biotite) and plagioclase were performed at the Departamento de Geología, Universidad de Chile, using a CAMECA SU-30. Additional analyses on sulphide and oxide phases were performed at ZELMI Laboratory, TU-Berlin, using a CAMEBAX microbeam, with PAP correction.

$^{40}Ar/^{39}Ar$ dating was carried out on separate amphibole (hornblende) grains from thick and thin mafic dikes. Approximately 1 kg of sample was crushed to obtain grain sizes of 100 to 250 μm. Amphibole separation was performed using an isodynamic magnetic separator and heavy liquids, followed by hand picking under a binocular microscope. The samples were irradiated in the nuclear reactor of the Comisión Chilena de Energía Nuclear (La Reina, Santiago de Chile). The irradiation factor for each sample was $J=0.0011009\pm8.500000e^{-6}$ (sample CC-03-01) and $J=1.03e^{-3}\pm7.900000e^{-6}$ (sample CC-03-13). Gas extraction was performed using a step heating procedure with a CO_2 laser beam on hornblende grain populations (<15 grains) in the Laboratorio de Geocronología of Servicio Nacional de Geología y Minería (SERNAGEOMIN). Detailed analytical procedures are given in Arancibia et al. (2006). The criteria used to define a plateau age is that it should contain more than 50% released ^{39}Ar, that there should be at least three successive steps in the plateau, and that the integrated age of the plateau should agree with each apparent age of the plateau within a 2σ error.

Sampling for AMS and paleomagnetic studies was carried out using an oil-powered drill at 15 sites. Samples were oriented using solar and magnetic compasses. Depending on dike thickness, 4 to 15 cores were sampled for each site. The Anisotropy of Magnetic Susceptibility (AMS) of the samples was measured and

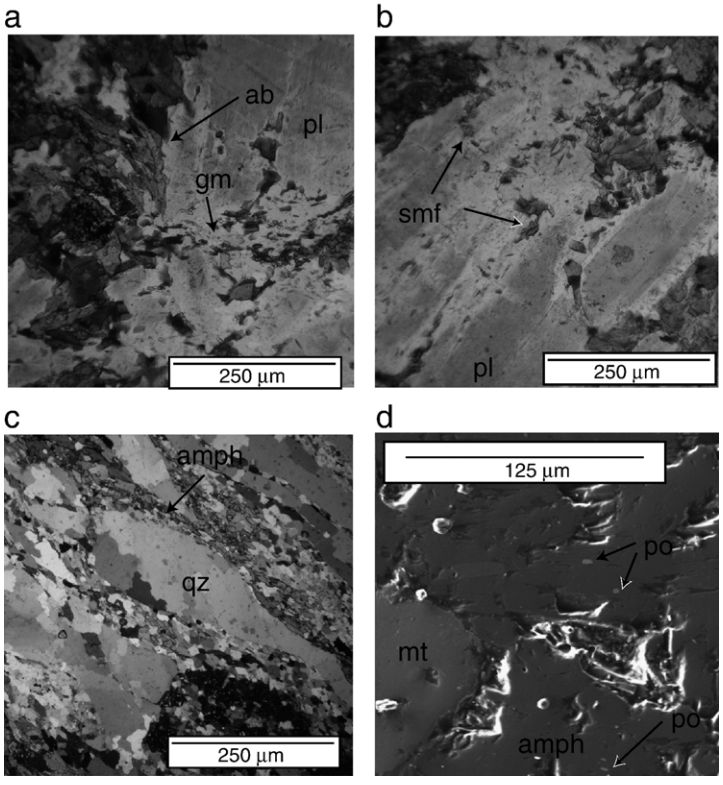

Fig. 4. a) Microscopic photograph under plane polarized light of a thick dike. Texture is characterized by several plagioclase phenocrysts (pl) with albitic rims (ab) surrounded by a bended and fine-grained groundmass (gm) composed mainly of amphibole, magnetite plagioclase, titanite and minor quartz (sample CC-03-06, plane polarized light) b) submagmatic filling (smf) of high-temperature minerals in plagioclase cracks (sample CC-03-06, plane polarized light) c) high-temperature solid-state foliation on a sinistral shear zone in tonalitic country rock near dike site RN05 (crossed polars). d) Secondary electron image in sample CC-03-56 from site 03RN13. Symbols are for amphibole (amph), magnetite (mt) and pyrrhotite (po).

Table 2
Detailed $^{40}Ar/^{39}Ar$ results on amphibole from the CMDS, Coastal Range, central Chile

Step	Atmospheric contamination	^{39}Ar(%)	$^{40}Ar/^{36}Ar$	$^{40}Ar/^{39}Ar$	Ca/K	$^{40*}Ar/^{39}Ar$	Age
Amphibole sample CC-03-01							
3-A	0	1.5	313.0448	792.2938	4.6938	56.8357	109.75±17.72
10-B	3.4	17.4	1131.7589	113.9389	20.1518	86.6393	164.74±1.60
13-C	23	48.9	4146.3060	88.3596	25.8551	85.4158	162.51±1.11
15-D	21.7	19	4148.1321	90.1398	27.4964	86.4207	164.34±1.29
20-E	25.8	11.4	4829.0370	89.1210	28.1028	86.3378	164.19±1.96
30-F	6.8	1.8	1433.0909	67.3675	18.6868	55.1434	106.57±6.64
Integrated Age=							162±3
(●) Plateau Age=		96.7					164±3
Amphibole sample CC-03-13							
3A	0.1	1.2	393.1015	215.1543	3.9012	56.5618	102.26±4.00
8B	1.1	6	1014.5854	140.7716	8.8848	101.5207	179.61±1.22
10C	8.7	13	3851.2137	97.4708	12.8312	91.51633	162.68±0.87
12D	18.6	29.1	6220.7283	92.7826	16.1312	90.1425	160.35±0.98
13E	11.4	15.9	4393.6934	95.0926	14.4218	90.3379	160.68±0.53
14F	14.6	7.7	5776.8367	92.7474	13.6807	89.5712	159.38±0.94
18G	13.6	19.8	4266.4746	95.6148	17.6907	90.9309	161.70±0.62
24H	8.1	6	3250.6197	97.5461	14.0656	90.3877	160.77±1.60
30I	11	1.3	4216.6667	99.0215	15.3655	93.7368	166.46±3.93
Integrated Age							161±2
(●) Plateau Age=		92.8					161±3

thermomagnetic experiments were conducted at the Laboratorio de Paleomagnetismo, Departamento de Geología, Universidad de Chile, using KLY-3S Kappa-bridge equipment (AGICO Ltd.), working under a weak alternative magnetic field, with a resolution as high as 10^{-8} SI. Additional measurements of IRM (isothermal

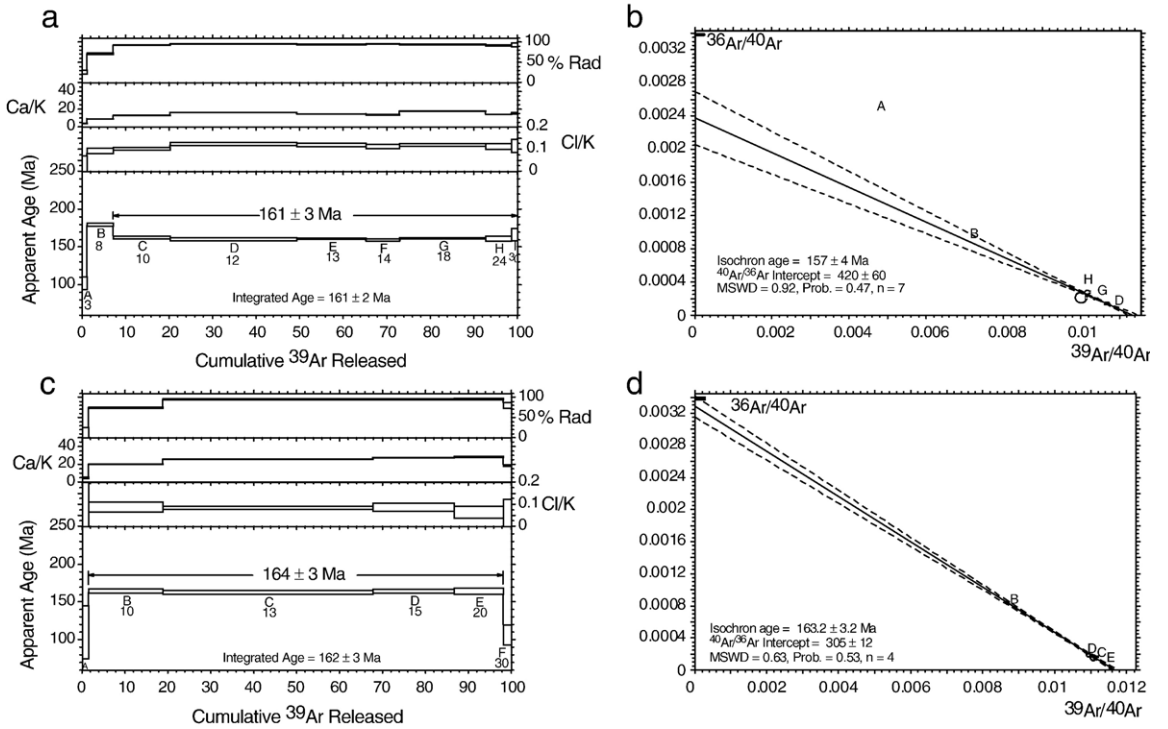

Fig. 5. a) Ar–Ar age spectra (plateau age) for sample CC-03-13 (thick dike) b) Inverse isochron for the same sample. c) Ar–Ar age spectra (plateau age) for sample CC-03-01 (thin dike) and d) inverse isochron for the sample.

Table 3
Location of AMS/paleomagnetic sampling sites and key field features from the CMDS and its country rocks, Coastal Range, central Chile

	Rock type	Strike/dip *granite foliation*	Thickness	Latitude	Longitude
03RN01	*Foliated granitoid*	324/86°SW		−32°55.489′	−71°32.650′
03RN02	*Thick dike*	297°/85SW	7 m thick	−32°56.288′	−71°33.029′
03RN03	*Thick dike*	307°/80°SW	9 m thick	−32°56.260′	−71°33.100′
03RN04	*Foliated granitoid*	1°/90°		−32°56.260′	−71°33.100′
03RN05	*Thick dike*	329°/90°	2–3.5 m thick	−32°55.756′	−71°32.889′
03RN06	*Foliated granitoid*	342°/90°		−32°55.756′	−71°32.889′
03RN07	*Thick dike*	330°/90°	4.3 m thick	−32°57.605′	−71°32.785′
03RN08	*Foliated granitoid*	340°/84°SW		−32°57.605′	−71°32.785′
03RN09	*Thick dike*	328°/90°	3 m thick	−32°57.605′	−71°32.785′
03RN10	*Thin dike*	300°/78°SW	1.2 m thick	−32°57.389′	−71°32.779′
03RN11	*Foliated granitoid*	332°/76°SW		−32°57.389′	−71°32.779′
03RN12	*Thin dike*	300°/78°SW	0.9 m thick	−32°57.389′	−71°32.779′
03RN13	*Thin dike*	303°/85°SW	0.7 m thick	−32°58.299′	−71°32.630′
03RN14	*Thick dike*	300°/75°SW	12 m thick	−32°58.299′	−71°32.630′
03RN15	*Granitoid*			−32°58.299′	−71°32.630′

remanent magnetization) were taken at the University of Rennes.

Remanent magnetization was measured with a Molspin or Agico JR5A spinner magnetometer. Magnetic susceptibility was measured with a Bartington susceptibilimeter. These measurements were performed on at least one specimen from each core at all sites. All of these measurements were performed at the Laboratorio de Paleomagnetismo, Departamento de Geología, Universidad de Chile.

5. The Concón mafic dike swarm and its host granitoids

5.1. Structural data and petrofabrics of the CMDS

The Concón Mafic Dike Swarm (CMDS) consists of basaltic to andesitic dikes that are exposed over a distance of 10 km along the coast between the localities of Concón and Reñaca (Fig. 1c). This swarm is composed of more than 60 individual intrusions. The intrusions are separated into two groups of dikes based on their field and petrographic features: thick dikes and thin dikes (Fig. 2).

Thick dikes are tabular bodies 5.5 to 12 m thick (Figs. 2 and 3a), oriented 284–328°/53–90° SW and characterized by a porphyritic texture with large plagioclase phenocrysts. They are weakly to moderately foliated in the field. The foliation, observed in plan view, is defined mainly by the orientation of feldspar crystals, and is usually 11 to 35° clockwise oblique of dike trend. All thick dikes show penetrative foliation at their margins, parallel to the dike trend. Xenoliths of foliated granitoids are common and some of them show a sigmoidal (sinistral) shape with an internal foliation parallel to those observed in the host dikes. Dikes branching from the main body are locally observed pointing to the NW and could indicate magma flow from SE to NW. Thick dikes contain normally zoned, large plagioclase porphyroclasts (cores: $An_{58–44}$, rims: $An_{24–18}$), in a dynamically recrystallized groundmass composed of a fine-grained oriented intergrowth of Mg-

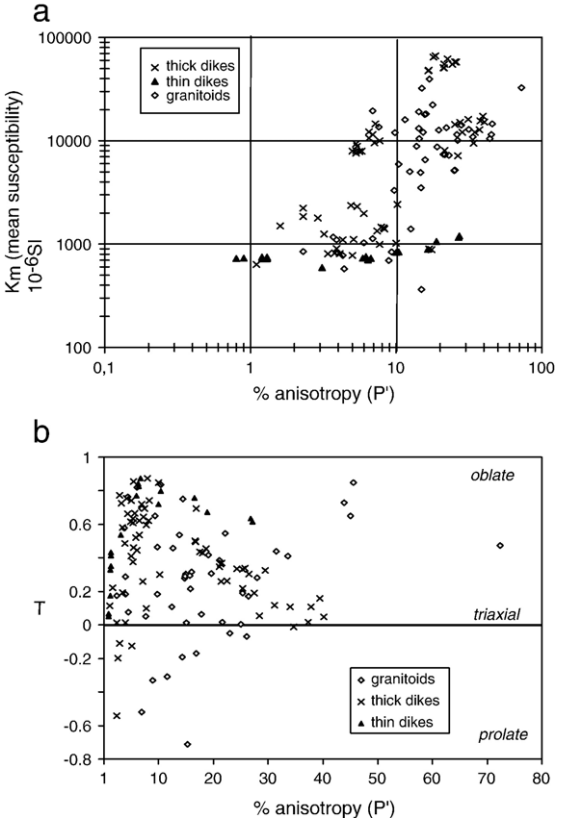

Fig. 6. a) K_m (mean susceptibility) vs $\%P'$ (anisotropy degree) b) $\%P'$ vs T (shape parameter) parameters for both dike types and country rocks.

Table 4
AMS data of dikes and granitoid country rocks

	Km (10^{-6} SI)	P'	T	K_1		K_2		K_3		L	F
				dec	*inc*	*dec*	*inc*	*dec*	*inc*		
Thick dikes											
03RN0207A	904	1.039	0.014	146.6	39.3	114.5	−46	42.5	16.6	1.019	1.019
03RN0206B	1250	1.032	0.726	158.8	39.8	94.6	−27.6	28.6	37.8	1.004	1.025
03RN0205A	14600	1.072	0.644	345.1	−1.9	261.2	72.4	74.5	17.5	1.012	1.055
03RN0201A	1100	1.043	0.662	300.2	20.6	152.6	66	34.7	11.8	1.007	1.033
03RN0202A	1980	1.06	0.444	137.3	42.2	119.8	−46.4	39.2	8.8	1.016	1.041
03RN0203A	7170	1.265	0.302	144.8	24.7	127.4	−64.2	51.6	6.8	1.084	1.163
03RN0204A	2420	1.102	0.299	139.8	52.2	116.3	−35.4	34.6	11.5	1.034	1.064
03RN0301A	885	1.175	0.436	126.1	7.2	307.4	82.8	216.1	0.2	1.045	1.119
03RN0302A	9490	1.34	0.109	149.2	10.9	336.8	79	239.4	1.4	1.139	1.176
03RN0303A	12100	1.284	0.054	150.4	10	150.3	−80	60.4	0	1.125	1.141
03RN0304A	15200	1.402	0.049	147.4	10.6	142.1	−79.4	57.2	1	1.174	1.194
03RN0305A	12800	1.373	0.015	155.2	11.2	148.7	−78.7	65	1.3	1.169	1.175
03RN0306A	12100	1.346	−0.013	150.5	7.9	119	−80.7	59.8	4.8	1.162	1.158
03RN0313A	15600	1.378	0.108	139.6	2.1	336.9	87.8	229.6	0.7	1.153	1.194
03RN0307A	17300	1.394	0.158	162.2	7.1	149.2	−82.7	72	1.6	1.149	1.211
03RN0308A	16100	1.312	0.117	166.6	8.2	160.6	−81.8	76.5	0.9	1.127	1.163
03RN0309A	15100	1.274	0.189	157.9	2.3	152.4	−87.7	67.9	0.2	1.103	1.154
03RN0310A	14400	1.253	0.217	152.6	1.4	150.1	−88.6	62.6	0.1	1.092	1.146
03RN0311A	8060	1.215	0.37	333.1	5.5	325	−84.5	243.1	0.8	1.062	1.139
03RN0312A	1020	1.1	0.85	324	18.3	144.7	71.7	54.1	0.2	1.006	1.083
03RN0314A	896	1.168	0.694	313.2	6.9	195.7	75.3	44.8	12.9	1.022	1.13
03RN0501A	994	1.077	0.597	342	−38.2	350.8	51.4	75.4	−4.3	1.014	1.058
03RN0501B	777	1.05	0.742	351.8	−15.9	25.6	71.1	84.7	−10	1.006	1.04
03RN0502A	822	1.038	0.485	352.4	−12.4	54.1	65.2	87.2	−21.1	1.009	1.027
03RN0502B	807	1.034	0.58	345.7	−16	42.6	62.3	82.4	−22	1.007	1.025
03RN0503B	809	1.041	0.754	345.8	−17.6	36.5	63.5	82.2	−19.2	1.005	1.033
03RN0504A	805	1.034	0.192	343.8	−47	5.3	40.9	85.7	−10.9	1.014	1.02
03RN0506B	1110	1.051	−0.124	154.4	40	188.8	−44.5	80.2	−17.9	1.028	1.022
03RN0705A	1790	1.029	−0.11	101.5	18.7	52.5	−62.7	4.8	19.1	1.016	1.013
03RN0702A	2230	1.023	−0.541	157.6	67.1	42.6	10.1	308.8	20.3	1.017	1.005
03RN0702B	1850	1.023	0.013	344.5	−51.8	5.4	36.3	87.8	−10.2	1.011	1.012
03RN0703B	1500	1.016	0.222	27.3	−58	301.9	2.9	33.7	31.9	1.006	1.01
03RN0704A	2310	1.054	0.461	150.5	69.1	59.7	0.3	329.6	20.9	1.014	1.038
03RN0704B	2370	1.049	0.615	173.1	68.6	64.4	7.2	331.8	20.1	1.009	1.037
03RN0904A	50800	1.213	0.364	354	21.9	151.2	66.4	80.6	−8.2	1.062	1.137
03RN0904B	51000	1.211	0.348	353.5	22.6	150.6	65.7	79.9	−8.5	1.063	1.135
03RN0903A	47600	1.166	0.502	353.9	33.1	152.5	55	77.3	−10.1	1.037	1.117
03RN0903B	48200	1.167	0.497	356.5	34.7	155.4	53.4	79.4	−10.2	1.038	1.118
03RN0905A	64700	1.18	0.428	348	17.1	151.3	72.2	76.5	−4.8	1.047	1.122
03RN0905B	66400	1.186	0.455	349.8	17.4	150.5	71.6	78	−5.7	1.046	1.127
03RN0906A	55200	1.214	0.26	360	22.7	164.8	66.6	87.6	−5.5	1.074	1.129
03RN0906B	62100	1.225	0.263	1.2	23.7	167.1	65.7	88.9	−5.3	1.077	1.135
03RN0902A	58100	1.253	0.331	353.1	21.7	158.4	67.6	81	−5.2	1.077	1.159
03RN0902B	58000	1.258	0.337	353.8	21.3	156.4	67.8	81.4	−6	1.078	1.163
03RN0901A	55100	1.243	0.334	355.3	23.6	155.1	65	81.9	−7.7	1.074	1.153
03RN1401A	1460	1.079	0.874	355.5	22.4	190.3	66.9	87.7	5.3	1.004	1.066
03RN1401B	1400	1.083	0.742	346.2	25	164	65	75.8	−0.8	1.009	1.066
03RN1402A	1340	1.074	0.695	342	52.2	180.8	36.3	84	9.1	1.01	1.058
03RN1402B	1440	1.082	0.623	351.7	19	183.8	70.6	83	3.8	1.014	1.062
03RN1403A	7950	1.058	0.52	18.4	8.1	158.5	79.5	107.4	−6.6	1.013	1.042
03RN1403B	7880	1.056	0.665	21.3	34.5	187.7	54.8	106.8	−6.4	1.009	1.043
03RN1404B	7620	1.053	0.635	20.5	25.6	171.5	61.3	104.6	−12.1	1.009	1.04
03RN1405A	9570	1.071	0.258	23.7	37	170.6	48	100.4	−17	1.026	1.044
03RN1405B	10000	1.077	0.1	24	32.9	168.6	51.6	102.1	−17.6	1.034	1.042
03RN1406A	8860	1.054	0.854	302.2	−84.7	359.9	2.8	89.7	−4.4	1.003	1.045

(continued on next page)

Table 4 (*continued*)

	Km (10^{-6} SI)	P'	T	K_1		K_2		K_3		L	F
				dec	*inc*	*dec*	*inc*	*dec*	*inc*		
03RN1407A	8030	1.053	0.377	4.3	28.1	162.8	60.1	89.3	−9.3	1.016	1.035
03RN1407B	7960	1.05	0.409	8.4	11.7	160.8	76.8	97.2	−5.9	1.014	1.034
03RN1408A	9370	1.053	0.609	354.4	−1.8	69.6	82.8	84.6	−7	1.01	1.04
03RN1408B	12200	1.065	0.538	2.3	−8.2	51.8	77.5	93.6	−9.4	1.014	1.047
03RN1409A	11500	1.069	0.72	334.9	−50.6	2.2	36.2	82	−13.6	1.009	1.054
03RN1409B	10600	1.065	0.622	143.8	61.9	169.7	−25.6	74.5	−10.7	1.011	1.049
03RN1410A	635	1.011	0.114	41.6	−51.8	338.3	19.5	80.8	31.4	1.005	1.006
Thin dikes											
03RN1001A	703	1.064	0.827	353.7	27.3	310.3	−54.6	252.4	20.7	1.005	1.053
03RN1001B	728	1.067	0.874	351.3	22.4	304.4	−58.9	252.5	20.4	1.004	1.055
03RN1002A	592	1.031	0.537	144.7	45.7	148.3	−44.2	56.6	−1.8	1.007	1.023
03RN1003A	730	1.059	0.769	344.9	28.7	150.8	60.6	71.6	−6	1.006	1.047
03RN1003B	756	1.062	0.841	348.6	27.5	151.6	61.4	74.9	−7.1	1.004	1.051
03RN1004A	840	1.104	0.798	342.5	26.7	324.8	−62.2	248.8	7.3	1.009	1.084
03RN1004B	1060	1.189	0.671	344.8	38.1	333.9	−51.4	250.6	5.3	1.027	1.144
03RN1201A	831	1.1	0.719	330.5	20.4	303.4	−67.4	237	9.5	1.012	1.079
03RN1202A	891	1.165	0.757	335.7	56.5	328.7	−33.3	240.8	3.2	1.017	1.131
03RN1203A	1200	1.271	0.614	334.5	46.5	159.9	43.3	67.4	2.7	1.045	1.2
03RN1203B	1160	1.268	0.633	336.4	49.9	156.5	40.1	66.5	0	1.042	1.199
03RN1301A	749	1.012	0.175	3.5	−64.8	325.4	20.3	60.8	14.2	1.005	1.007
03RN1301B	720	1.012	0.327	2.4	−63.9	330.7	22.7	66	12.3	1.004	1.008
03RN1302A	723	1.013	0.431	343.9	−53.2	322.9	34.9	60.1	10.1	1.004	1.009
03RN1303A	748	1.013	0.414	356	−56.8	328.2	30.1	65.7	12.8	1.004	1.009
03RN1303B	740	1.013	0.351	356.3	−54.9	336.5	33.5	72.8	9.4	1.004	1.009
03RN1304A	726	1.008	0.052	14.6	−62.6	331.8	20.9	68.5	17	1.004	1.004
03RN1304B	730	1.009	0.066	16.9	−61.2	326.4	19.3	64	20.6	1.004	1.005
Granitoids											
03RN0101A	14600	1.456	0.85	327.6	0.5	236	70.6	57.7	19.4	1.026	1.366
03RN0101B	11500	1.45	0.651	158.6	18.5	123.3	−67.7	64.5	12	1.063	1.332
03RN0102A	5150	1.25	0.003	163.8	37.6	141.9	−50.3	65.3	10.9	1.118	1.119
03RN0102B	5200	1.253	0.191	164.3	35.8	129.6	−48.7	61	17.7	1.095	1.143
03RN0103B	10500	1.439	0.73	163	33.5	134	−52.9	63.5	14.1	1.046	1.337
03RN0104A	12900	1.315	0.44	168.9	54.3	137.1	−31.4	56.6	15.2	1.077	1.211
03RN0104B	14200	1.28	0.281	166.6	52.6	137.2	−33.7	57	14.3	1.092	1.169
03RN0401A	18000	1.157	0.295	196	20	174.9	−68.7	103.4	7.1	1.052	1.098
03RN0401B	18200	1.16	0.316	9.2	−0.1	91.6	89.5	99.2	−0.5	1.051	1.101
03RN0402A	6550	1.158	0.215	349.8	−13.5	19.7	74.6	81.6	−7.4	1.059	1.093
03RN0402B	3510	1.148	0.29	346	−8.7	23.3	79.1	77	−6.5	1.049	1.092
03RN0403A	13600	1.076	0.052	187.3	53.8	169.1	−34.8	85.2	8.7	1.035	1.039
03RN0403B	12000	1.098	0.185	202.4	69.2	178.4	−19.2	91.2	7.8	1.038	1.056
03RN0404A	3310	1.097	0.463	358.4	−27.7	21	60.3	93.5	−9.7	1.024	1.068
03RN0405A	7400	1.211	0.386	356.5	15.2	205.2	72.8	88.6	7.9	1.066	1.128
03RN0405B	7350	1.216	0.015	179.1	27.2	170.8	−62.5	87.3	3.4	1.101	1.104
03RN0602B	39600	1.169	−0.171	130.3	47.2	106.8	−40.3	27.1	11.9	1.095	1.067
03RN0603A	32300	1.15	0.013	134.4	30.4	117.3	−58.5	39.9	7.6	1.072	1.074
03RN0604A	19500	1.069	−0.521	157.6	44.8	113.4	−35.8	41.8	23.7	1.05	1.015
03RN0605A	12700	1.196	0.306	137.7	38.8	353.1	45.4	243.3	18.5	1.063	1.122
03RN0606A	13200	1.143	−0.193	143.9	17	31.1	51.8	245.4	33.1	1.082	1.055
03RN0607A	5030	1.124	0.109	150.7	36.7	349	51.9	247.4	9	1.053	1.067
03RN0607B	12100	1.153	−0.713	139.3	16	25.7	54.3	239.2	30.9	1.119	1.019
03RN0608A	16000	1.115	−0.308	133.7	14.1	106.2	−74.1	42	7	1.073	1.038
03RN0609A	22300	1.178	0.063	151.1	40.3	129.1	−47.6	51.5	11.1	1.08	1.091
03RN0610A	19100	1.143	−0.193	149.1	37.7	339.2	51.9	242.9	5	1.073	1.086
03RN0611A	32700	1.724	0.474	352.9	1.9	274.6	−80.9	262.6	8.9	1.148	1.472
03RN0801A	1400	1.126	0.459	338.2	64.8	181.3	23.4	87.4	8.8	1.032	1.087

Table 4 (*continued*)

	Km (10^{-6} SI)	P'	T	K_1		K_2		K_3		L	F
				dec	*inc*	*dec*	*inc*	*dec*	*inc*		
03RN0802A	577	1.044	0.076	190.1	70.9	170.6	−18.1	82.6	6	1.02	1.023
03RN0802B	694	1.089	−0.329	214.2	75.1	143.9	−5.1	55.1	14	1.057	1.028
03RN0803A	364	1.149	0.304	349.4	−11.4	346.5	78.6	79.3	0.6	1.049	1.093
03RN0804A	10900	1.336	0.412	343.5	3.1	238.2	78.5	74.1	11	1.086	1.22
03RN0804B	4930	1.147	0.278	353.7	−25.5	3.7	64.1	85.6	−3.9	1.05	1.09
03RN0805A	10100	1.264	0.17	338.5	5.9	226.7	74.4	70	14.4	1.102	1.146
03RN0805B	7240	1.23	−0.049	349.2	−1	263	75.5	78.9	14.5	1.115	1.103
03RN0806A	10500	1.144	0.751	356.6	−14.2	319.1	72.3	84	10.3	1.015	1.114
03RN0806B	13400	1.221	0.545	353.1	−16.5	335.2	72.7	81.6	5	1.044	1.158
03RN0807A	11500	1.261	−0.069	347.4	2.7	246.9	75.2	78.1	14.5	1.132	1.114
03RN1101A	1030	1.06	0.819	121	55.4	336.4	29.4	236.7	16.7	1.005	1.05
03RN1102A	830	1.039	0.287	133.1	48.3	130.6	−41.7	41.7	1.2	1.014	1.025
03RN1103A	778	1.043	0.764	316.4	1.7	233.1	−76.1	226	13.8	1.005	1.035
03RN1104A	1130	1.069	0.693	156.4	36	154.6	−54	65.8	0.9	1.01	1.053
03RN1105A	1170	1.037	0.579	338.1	21.4	275.2	−49.4	233.5	32.7	1.007	1.028
03RN1106A	1100	1.039	0.185	146.7	18.6	342.8	70.7	238.4	5	1.016	1.023
03RN1107A	847	1.023	0.173	323.6	−39.3	337.2	49.9	59.1	−6.7	1.009	1.013
03RN1501B	8720	1.191	0.417	167	31.7	155.7	−57.8	73.8	5.1	1.051	1.128
03RN1502A	5940	1.104	0.835	166.8	68.1	154.9	−21.5	66.5	4.1	1.007	1.085
03RN1502B	8860	1.138	0.536	344.4	10.6	177.3	79.1	74.8	2.4	1.029	1.1
03RN1504A	840	1.093	0.65	162.8	72.3	153.6	−17.5	64.5	2.6	1.015	1.071

Samples of dikes are listed from SW to NE margin.

hornblende, Na-plagioclase, and minor quartz and magnetite rimmed by titanite. These grains are commonly bent around large plagioclase porphyroclasts (Fig. 4a). We estimated high recrystallization temperature, between 620 and 690 °C from geothermometric calculations, using the compositions of amphiboles and coexisting plagioclase rims (Holland and Blundy, 1994). The presence of plagioclase porphyroclasts with fractures filled with minerals similar to those observed in the groundmass suggests submagmatic flow during deformation (Fig. 4b, Paterson et al., 1989; Bouchez et al., 1992).

Thin dikes are 0.5 to 3 m thick (Figs. 2 and 3b) and oriented 274–320°/50–90°SW. Some of them are observed cutting thick dikes. These dikes also have a well developed foliation oriented in a direction clockwise to the dike margins. Penetrative foliation is also present at the margins, but parallel to the dike trend. Minor xenoliths of granitoids are also present; some of them show a sigmoidal shape in vertical view, suggesting subvertical shearing during dike emplacement (Fig. 3b). The microfabrics of thin dikes are created by an equigranular arrangement of fine-grained plagioclase ($An_{56–45}$), Mg-hornblende, titanite and magnetite. Foliation is clearly observed in thin sections but does not shows effects of solid-state deformation, such as generation of submagmatic microcracks or ondulose extinction. This is consistent with the magmatic temperatures of about 700 °C obtained from geothermometric calculations in hornblende–plagioclase pairs (Holland and Blundy, 1994).

5.2. Structural data and petrofabrics of granitoid country rocks

In the study area, granitoid country rocks are polydeformed. The main tectonic fabric is characterized by a solid state foliation (315–360°/72–90° S, Fig. 1) and a southward-plunging stretching lineation (167–175°/42–50°), both defined by the orientation of mafic minerals, feldspar phenocrysts and mafic enclaves where present. Feldspars and mafic minerals are ductily deformed. Amphibole phenocrysts vary in composition between ferro-edenite, ferro-pargasite and hastingsite (locally ferro-tschermakite). These minerals are characterized by a slight decrease in Ti content from core to rim, where the cores probably represent magmatic compositions, and the borders are characterized by small dynamically recrystallized grains associated with small rutile grains. Plagioclase in most cases corresponds to andesine ($An_{32–30}$). Estimations of equilibrium temperature for this fabric, using the geothermometer of Holland and Blundy (1994) in hornblende–plagioclase pairs indicate that this deformation occurred at high temperatures between 610 and 665 °C (assuming a pressure of 3.5 kbar; Arce, 2002). These calculations, coupled with the microscopic observations, suggest that

the granitoids were deformed at high temperature (amphibolite facies, following models of Simpson, 1985).

Discrete shear bands (<20 cm thick) are another common deformational feature observed in the granitoids in the vicinities of some thick dikes. These structures are characterized by a foliation oriented 18°–0°/~90° and C shear planes oriented 320°–342°. The micro fabrics consist of an arrangement of ductily deformed quartz, feldspars, amphibole and biotite (Fig. 4c). Quartz ribbons display sinistral kinematic indicators, consistent with the arrangement of S and C planes. Some of the sinistral shear bands are intruded and displaced by thin dikes. Dextral shear bands (23°–30°/90°) are locally observed, displacing thin dikes. Scarce lineations in these dextral bands are subhorizontal.

5.3. Geochronology

Separated amphibole (hornblende) grains from the groundmass of the samples (thick dike sample CC-03-13; thin dike sample CC-03-01) were dated by $^{40}Ar/^{39}Ar$ dating. Analytical results are given in Table 2. For thick dikes (sample CC-03-13) a plateau age of 161±3 Ma (92.8% of ^{39}Ar released, Fig. 5a) was obtained on hornblende from the deformed groundmass. However, an inverse isochron indicates a component of excess ^{40}Ar in this sample. The corrected age for the sample is 157±4 Ma (Fig. 5b). For a thin dike (sample CC-03-01), a plateau age of 164±3 Ma (96.7% of ^{39}Ar released) on magmatic hornblende was obtained (Fig. 5c). The isochron age for this sample (163±3.2 Ma) on which $^{40}Ar/^{36}Ar$ intercepts near the atmospheric ratio (Fig. 5d), is similar to the plateau age.

According to the textural relationships of hornblende grains in both kinds of samples, and given the closure temperature for the $^{40}Ar/^{39}Ar$ in amphibole (450°–525 °C), we interpret the age obtained in the thick dike (sample CC-03-13) as the minimum age for a deformation event (well developed in the groundmass of the sample) that occurred close to time of dike emplacement. In the thin dike (sample CC-03-01), the age obtained represents cooling after emplacement and development of the magmatic fabric of the rock. Although the age of the thin dike is slightly older than that of the thick dike, both ages are within the same uncertainty limits and are consistent with field evidence that both dikes were emplaced during a common geological event.

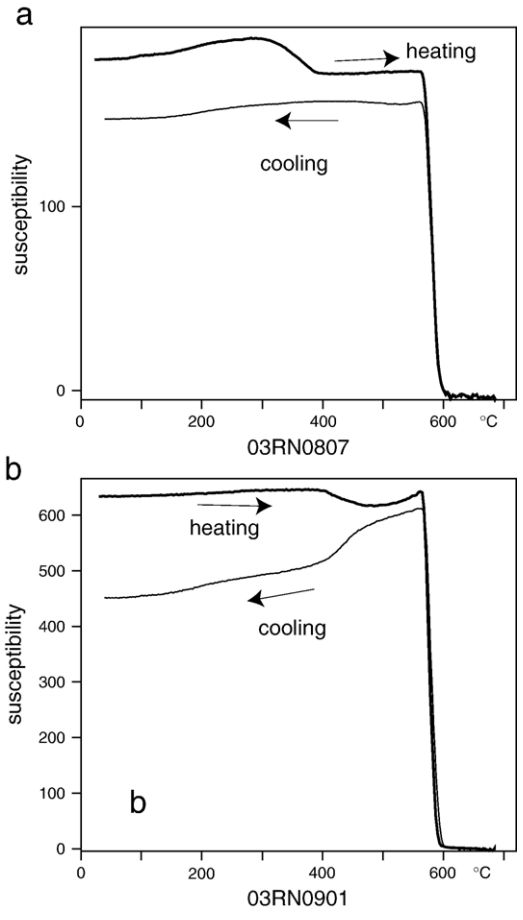

Fig. 7. Variation of magnetic susceptibility versus temperature in representative specimens of granitoids (a, b, c, d) and thick dikes (e, f).

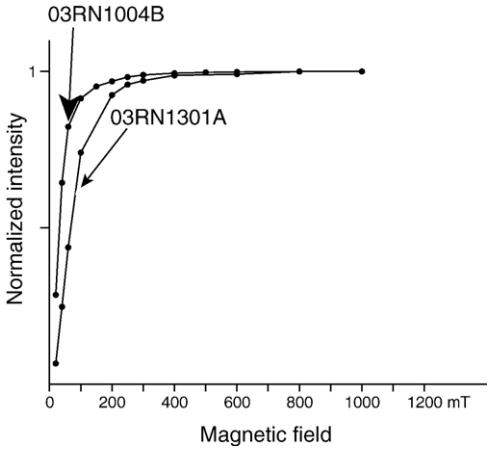

Fig. 8. Acquisition of isothermal remanent magnetization (IRM) showing rapid increase of magnetization typical of magnetite in samples RN1004B and RN1301A.

6. AMS fabrics

Sampling was carried out at 15 sites (six from granitoid country rocks, six from thick dikes and three from thin dikes, Table 3). Four to 15 cores were sampled

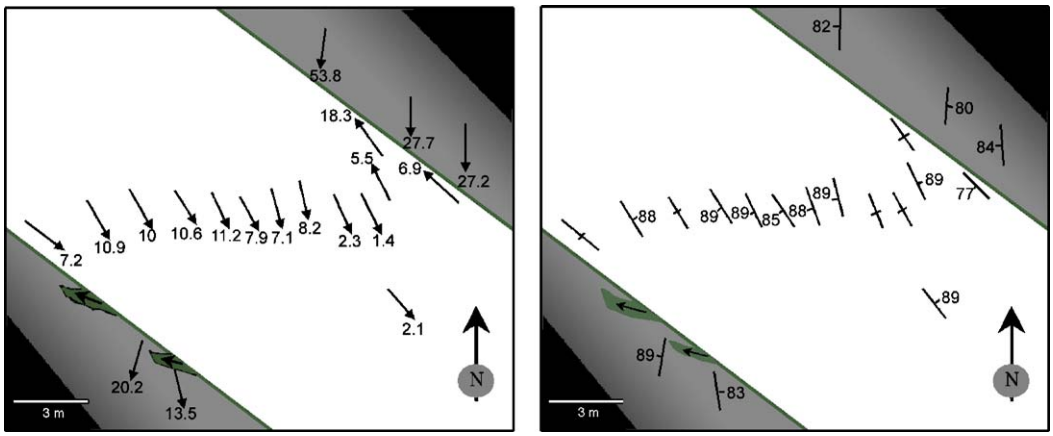

Fig. 9. Geological sketch of the arrangement of magnetic foliation and lineation in a thick mafic dike site (03RN03) and granitoid country rock (site 03RN04), showing the presence of an asymmetrical fabric.

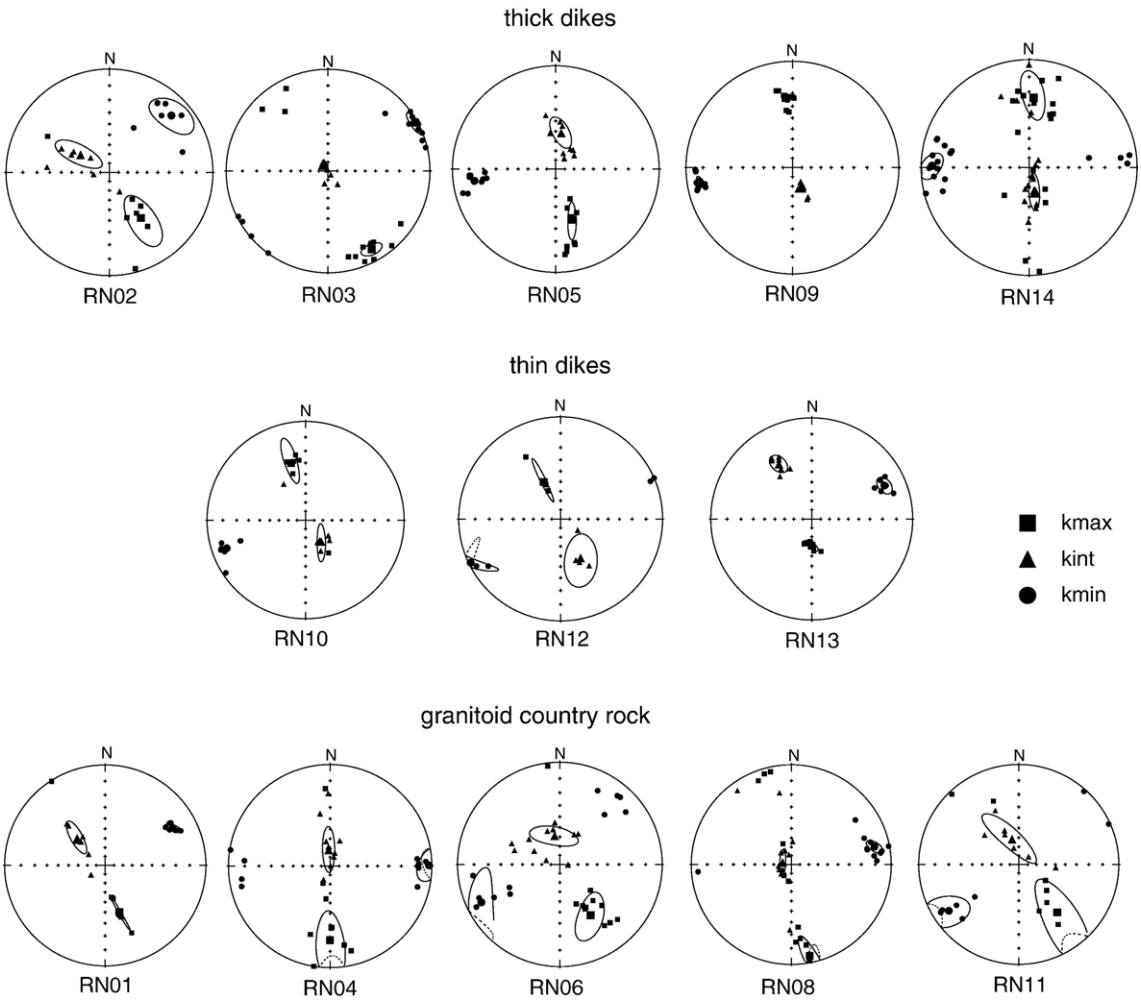

Fig. 10. AMS plots for thick dikes, thin dikes and granitoid country rocks.

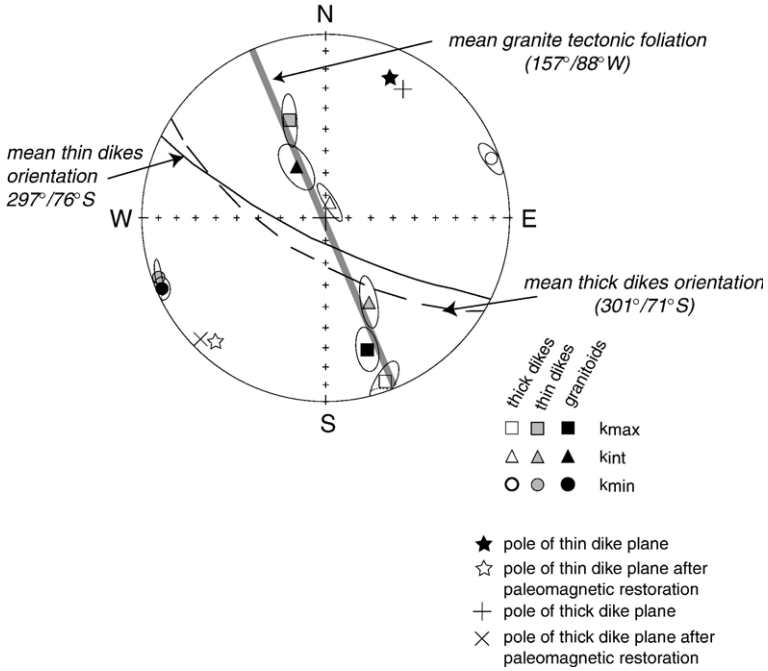

Fig. 11. Tensorial mean AMS vectors K_1, K_2 and K_3 for dikes and country rocks. Key field structures are also plotted. Pole of thin and thick dikes mean orientation are plotted as an example of the restoration of rotations.

for each site. Sampling of the dikes was performed along strike of the intrusions where we suppose we can observe major variations on the fabric of the dikes. Flow directions in dikes derived from AMS data are better defined near the chilled margins where elongate and planar particles become imbricated (Knight and Walker, 1988; Tauxe et al., 1998). For this reason, the sampling for AMS analyses should be performed as close as possible to the dike margins. However, in the present study, the AMS fabric is a result of tectonic deformation combined with magma flow. Moreover, in aphanitic dikes it is not easy to accurately observe effects of deformation or magmatic flow.

6.1. Magnetic properties and magnetic mineralogy

Thick dikes and granitoids show ferromagnetic behaviour, with $K_m > 500e10^{-6}$ SI (Fig. 6a, see Table 4). Some show strong ferromagnetic behaviour, with K_m up to $47000e10^{-6}$ SI (dike site RN09) and up to $32000e10^{-6}$ SI (some samples of granitoid site RN06). In some thick dikes, we observed K_m varying from low susceptibility at the margins (generally between 635 and $890e10^{-6}$ SI) to higher values in the centres (generally higher than $1000e10^{-6}$SI). Thermomagnetic experiments show Curie points between 570 and 580 °C for selected samples of granitoids and thick dikes (Fig. 7a and b respectively). This implies the presence of low-Ti magnetite as the main ferromagnetic phase.

Thin dikes always show weak ferromagnetic behaviour (Fig. 6a; mean K_m of all three sites = $813e10^{-6}$SI). Thermomagnetic curves in thin dikes do not show a well defined pattern in the variation of K, mainly because of their low susceptibility. However, IRM (isothermal remanent magnetization) experiments in two specimens of

Table 5
Paleomagnetic results of Middle Jurassic dikes

Site	*Unblocking T* °C	*n*	*D*°	*I*°	α_{95}	*k*
Component A±B						
RN12±10	260–360	4	341.4	−16.8	6.9	180
RN13	260–360	3	349.4	−32.1	7.3	289
RN05	260–360	3	337.7	−33.3	9.8	159
RN14	500–610	4	173.1	30.1	4.7	378
RN07-C1	500–580	5	334.0	−33.9	9.7	63
Mean		5	343.2	−29.4	9.4	*67*
Component C						
RN02	210–460	7	346.1	−57.9	6.7	83
RN03	210–490	13	355.0	−57.3	3.7	125
RN05	210–530	4	351.0	−56.0	4.5	422
RN07-C3	210–500	6	340.8	−53.0	6.2	118
RN14	210–500	7	354.4	−53.4	3.6	279
Mean		5	349.4	*−55.6*	3.9	*391*

thin dikes (site RN10 and RN13) indicate rapid saturation of magnetization residuals with the applied field (Fig. 8). This saturation curve suggests the presence of magnetite. Detailed microprobe analyses indicate the presence of rare grains of low-Ti magnetite in samples of site RN13 (Fig. 4d). The main sulphide phase in the samples appears to be pyrite, but small amounts of pyrrhotite were also detected, mainly as rounded inclusions within unaltered calcic amphibole (Fig. 4d). This observation suggests that pyrrhotite is a primary

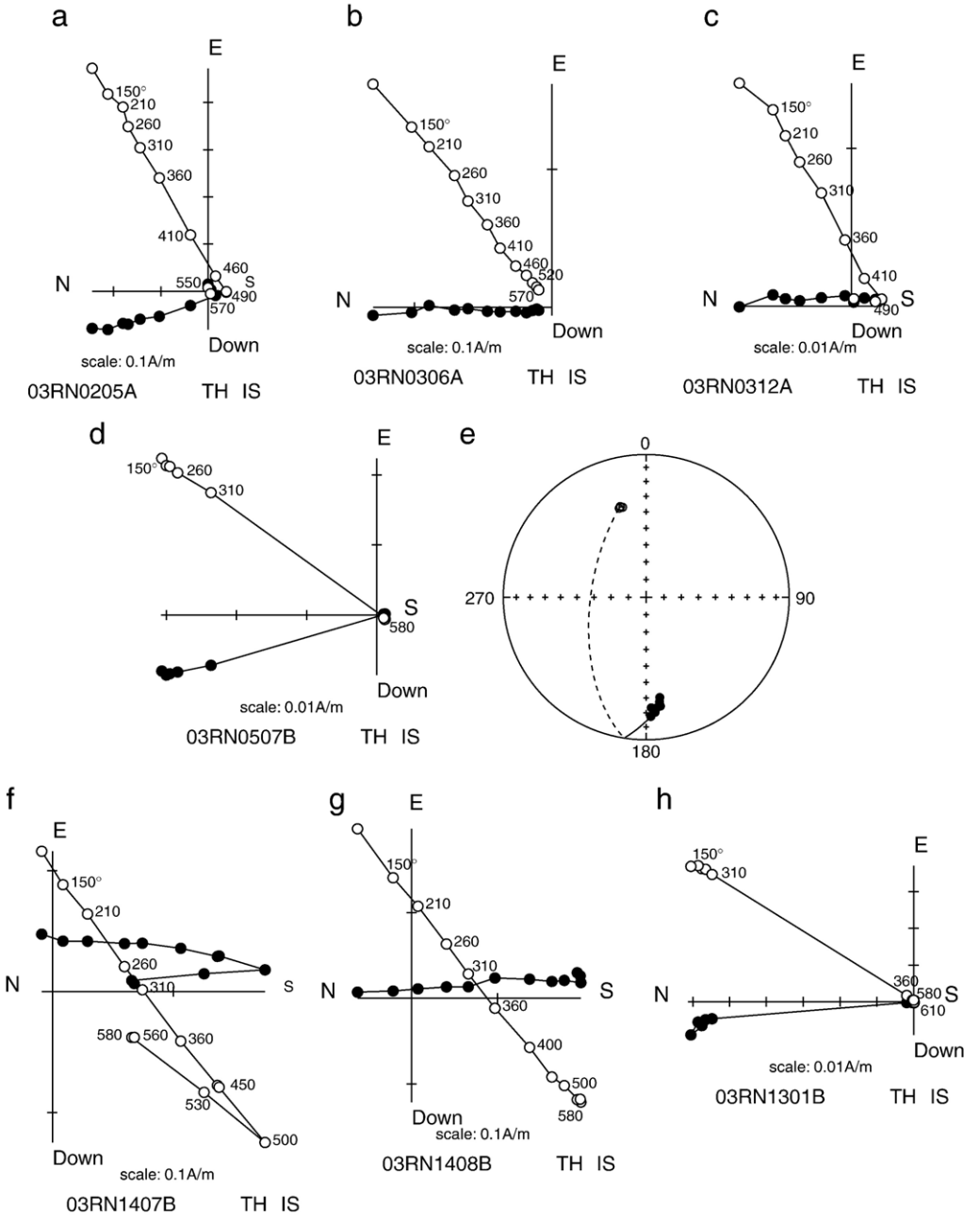

Fig. 12. a, b and c) Representative curves of demagnetization in orthogonal projection for samples of thick dikes. d) orthogonal projection of demagnetization diagram of a sample of a thin dike within a site of thick dikes (RN05) and e) equal-area projection of paleomagnetic directions from this sample. f) Orthogonal projection of demagnetization diagram (on right, 10 g) for a sample of a thin dike (03RN1301B), demonstrating the presence of magnetization with an unblocking temperature near 320 °C. h and i) orthogonal projection of demagnetization curves for samples of site RN14, intruded by thin dikes, showing the presence of a component of magnetization of reverse polarity at high temperature (>500 °C).

phase in the samples. The amount of magnetic phases, such as magnetite and pyrrhotite, in thin dikes is low, in agreement with the low magnetic susceptibility of the samples (Fig. 6a) and the behaviour of the hysteresis loop, showing clear signs of paramagnetic phases in the experiments (not shown).

6.2. Scalar and directional data

Granitoids and dikes are dominated by oblate ellipsoids and a variable degree of anisotropy (P'), but are generally lower than 8% (Fig. 6b). Triaxial ellipsoids noted in some granitoids (site 06) are correlated with poorly-developed foliation observed in the field for these sites. High P' (>20%) is observed in more deformed samples, such as mylonitized thick dikes (site RN03), strongly foliated thin dikes (RN12), and granitoids (RN01 and locally in RN06). The thick dike at site RN03 shows strongly oblate (T between 0.69 and 0.85) ellipsoids with lower K_m and %P at sheared margins and weakly oblate to prolate ellipsoids in central parts (Table 4). These more oblate ellipsoids at margins appear to be contradictory with a higher shear strain, where prolate ellipsoids are expected. An explanation for this is a mineralogical control of the fabric. The sheared margins having lower phenocryst concentration (more aphanitic) and consequently lower K_m probably do not record a stronger fabric than the crystal-rich dike centers, that have facility to register minor increments in deformation and in this case show more intense AMS fabric parameters (%P and prolate ellipsoids).

The most noticeable feature of the AMS data in the dikes is the presence of oblique fabrics at all sites (Fig. 9). This feature is particulary well observed in thick dikes, where magnetic foliation at the margins tends to be parallel to the dike trend, but is oriented 10 to 40° clockwise of the trend in the central parts, thus producing a sigmoidal pattern of foliations. Thick dikes with a high percentage of anisotropy (RN03 and RN09) are characterized by vertical foliation planes and lineations that plunge gently to the south (Figs. 9 and 10). Thick dikes with a lower percentage of anisotropy show more variable plunges of magnetic lineation to the south (Fig. 10). In thin dikes, the plane of magnetic foliation is nearly vertical and lineations plunge steeply to the north. Another outstanding feature is the similarity observed between magnetic foliations in dikes and associated country rocks. This is clearly observed in tensorial site-mean magnetic vectors (Fig. 11). For granitoid country rocks, oblate ellipsoids are dominant and AMS directional data correlates well with structural elements measured in the field (foliation and lineation).

7. Paleomagnetic results

A study of the remanent magnetization and thermomagnetic behaviour of the rocks was performed on at least one specimen from each core at all sites. For

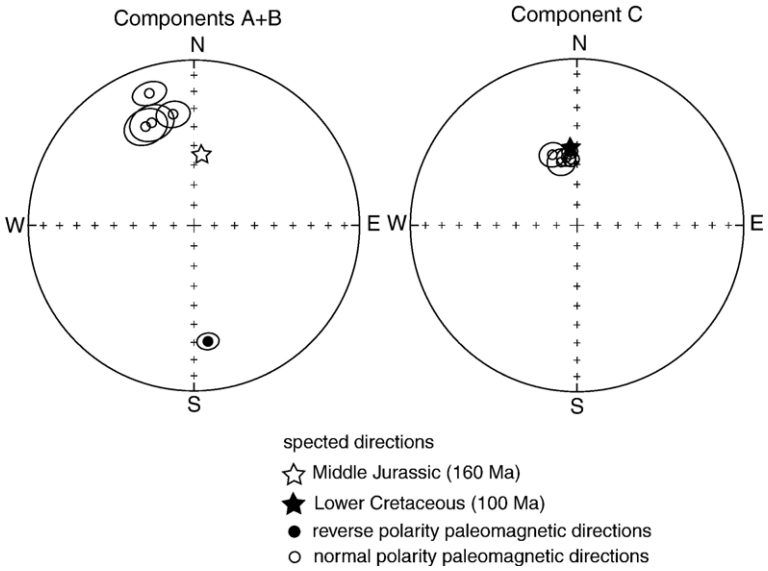

Fig. 13. Equal area projection of site mean directions for dikes and granitoids. Expected directions for Middle Jurassic and Early Cretaceous calculated from the APWP of Besse and Courtillot (2002). Open circles represent normal polarity directions and black circles represent reverse polarity directions.

calculations of tectonic rotations, we used the reference poles derived from the Apparent Polar Wander Path (APWP) of Besse and Courtillot (2002). Details of this study are given by Arriagada et al. (2003). Mean-site directions are listed in Table 5.

A magnetization of normal polarity is observed for the majority of thick dikes and country rocks during thermal demagnetization in the temperature range 210–530 °C (Fig. 12a, b, c; component C in Table 5). In general, these paleomagnetic directions are roughly homogeneous (Fig. 13) and are very similar to those published by Irwin et al. (1987) for Mesozoic coastal mafic dikes.

Magnetization of normal polarity with a weak inclination (ca. 15 to 20° lower than the inclination expected for stable South America during the Jurassic) is observed in thin dikes (Fig. 12d, e and h, component B in Fig. 13 and Table 5). This magnetization is associated with a very definite unblocking temperature between 320 and 360 °C (Table 5), that represents the Curie temperature of pyrrhotite, the probable carrier of this low-temperature magnetization. In the same samples, a poorly defined magnetization of inverse polarity and low inclination is observed at a high temperature between 500 and 610 °C (component A in Table 5, Fig. 12e). These magnetization temperatures, coupled with the results of IRM experiments, suggest that the small amounts of primary low-Ti magnetite recognized in the samples (Fig. 4d) are the carriers of this magnetization. These particular paleomagnetic directions are also observed in thick dikes and country rock granitoids that are intruded by thin dikes (e.g. site RN14; Fig. 12f and g). At these sites of thick dikes and granitoids, changes in magnetic properties are also observed, mainly a decrease in magnetic susceptibility. Site 03RN11, intruded by thin dikes (sites 03RN10 and 03RN12) shows similar paleomagnetic directions around the thin dikes, with a low inclination (45 to 13° N). Thick dike site 03RN14 shows paleomagnetic directions of inverse polarity at high temperature (>350 °C, Fig. 12f and g). These features strongly suggest that magnetization in thin dikes is primary and that the sites intruded by these rocks reflect changes in magnetic properties due to the localized effect of the intrusions.

8. Discussion

8.1. Origin and development of CMDS petrofabrics and magnetic fabrics

Asymmetrical fabrics, similar to those observed in the CMDS and characterized by foliation and lineation oblique to the trend of the dike, have been attributed to the intrusion along active transcurrent faults or fractures (e.g. Blumenfeld and Bouchez, 1988; Hutton, 1992; Correa-Gomes et al., 2001; Féménias et al., 2004). Therefore, this kind of fabric is developed under the influence of magmatic and tectonic stresses. Theoretical models of Correa-Gomes et al. (2001) attributed the pattern of asymmetrical internal dike fabrics (with foliations parallel to the dike along the margins and oblique in centers) as related to external stresses at least five times higher in magnitude than magma-flow-related stress. This excess of external stress, acting as a simple shear component, facilitates the development of wall-parallel shear planes (Blumenfeld and Bouchez, 1988) such as those observed in the dikes of the CMDS. This type of fabric is clearly distinguishable from fabrics developed under the influence of pure magma flow, which are characterized by a mirror imbrication of fabric with respect to the margin of the dikes (e.g. Johnson and Pollard, 1973; Tauxe et al., 1998; Geoffroy et al., 2002).

We have explored the correlation between magnetic and shape fabrics. In granitoid country rocks, where foliation and lineation were measured in the field, these show a very good correlation with AMS fabrics and the last one can be considered as representative of the petrofabric axes. In the case of thick dikes, in spite of a scarce dataset of field-measured foliations and lineations (mainly because of the incomplete exposure of dikes), AMS fabrics show a good correlation with the pattern of mineral alignment observed in the field. Microscopic examination of the samples demonstrated that magnetite grains, the main carrier of the magnetic signal, occurs in most cases as isolated grains (with a titanite rim), that are oriented parallel to the fabric of the deformed groundmass and the magnetic ellipsoid is controlled by shape anisotropy of magnetite, avoiding the presence of distributed anisotropy (caused by the interaction or clustering between magnetic grains that can cause a departure of the AMS ellipsoid from the shape fabric ellipsoid). In the case of thin dikes, a correlation between AMS directional data and field observations has also been observed. The weak ferromagnetic behaviour of the samples is probably controlled by the low contents of magnetite present in the samples, but we do not know at this point what are the magnetic effects on the AMS signal of sulphides or paramagnetic grains.

For the case of the CMDS, we suggest that magma emplacement and external (tectonic) stress were approximately contemporaneous because of their high-temperature (~solid state flow) to magmatic state microfabrics (Fig. 4a, b). These kinds of microfabrics are a common feature of syntectonic intrusions (e.g. Paterson et al.,

1989). The emplacement of thick dikes would have been controlled by and coeval with transcurrent sinistral shear along NW-trending structures, dipping 90–70° to the south. The horizontal component of displacement was dominant in the thick dikes, as denoted by the low plunge of magnetic lineation (Figs. 10 and 11). Thick dikes with a steeper southward-plunging lineation were probably associated with a more important vertical displacement along NW-trending structures. In the case of thin dikes, the dominant presence of steeply-plunging lineations suggests that vertical displacements were dominant (see also Fig. 3b) and we suggest that there was a minor change to transpressional conditions, with sub-vertical stretching.

The main tectonic fabric of the granitoids developed previous to the intrusion of the CMDS, as shown by the presence of already foliated granitoid xenoliths within some thick dikes. The high temperature conditions estimated for the fabric suggest that the timing was closer to the emplacement of the granitoids, during the Late Paleozoic. On the other hand, the formation of the discrete sinistral shear zones was coeval with the intrusion of the thick dikes, whereas NE-trending dextral shear zones were active shortly after intrusion of the late thin dikes, as suggested by the crosscutting relationships observed in the field. These discrete shear zones were probably produced as a way to accommodate in part the space created for the intrusions.

8.2. Origin of magnetizations and their tectonic significance

Differences in paleomagnetic directions observed in rocks of a single area can only be explained as the product of magnetization acquired during different geological times. In the study area, the differences in paleomagnetic directions between thick and thin dikes are consistent with differences in magnetic properties between these rocks and indicate that these magnetizations were acquired in different geological times.

We recognize three different components of magnetization in the CMDS. Components A and B are interpreted as primary features, present in thin dikes and their associated host rocks. Component C is present in thick dikes and some granitoid country rock sites and is considered to result from remagnetization during a later tectonic event. Unblocking temperatures for component A are characteristic of low-Ti magnetite present in the mafic dikes in small amounts. The second component of magnetization (B), of lower temperature and normal polarity, is carried by pyrrhotite that is a primary mineral included in amphibole (Fig. 4d). The characteristic directions of magnetizations A and B, of low inclination in high and low temperature can be explained by two mechanisms: a) broad displacement of the Chilean forearc towards the south after dike emplacement; b) regional block tilt towards the north of approximately 19–36° (with a mean of 23.2°, Table 5). The first hypothesis is not supported by previous paleomagnetic results in Mesozoic rocks of central Chile (Beck et al., 1986, 1990). Besides this, to explain this change in paleomagnetic declination, a north–south latitudinal transport of several thousand kilometres is needed. Such displacements would need to be explained by the presence of north–south structures in the forearc. Lateral displacements in large forearc structures in the central Andes are unable to explain such block movements (Grocott and Taylor, 2002; Arancibia, 2004; Cembrano et al., 2005). We thus favour the hypothesis of a regional tilt, which occurred after the CMDS was cooled below the Curie point of pyrrhotite (ca. 320 °C), during the Jurassic–Cretaceous. Several studies have demonstrated that block tilting is a common feature of extensional terranes (e.g. Karson et al., 1992; Irving et al., 2000). The changes in inclination were accompanied by minor vertical axis rotations of less than 15° (Fig. 13).

The block tilting process can best be explained by extension in a NNW–SSE direction, following the deviation in paleomagnetic directions (Fig. 13). If restoration of paleomagnetic rotations from the thin dikes is applied, assuming a mean change in inclination of about 23.2° to the NNW, the main attitude of thin mafic dikes changes from steeply inclined to the southwest (a dike pole of 27°/14°) to near-vertical (dike pole is translated to 221.8°/9.2°; Fig. 10). This restoration implies that the thin dikes were intruded originally in a near-vertical orientation and were then tilted to the NNW (Fig. 14). This restoration also can be applied to the thick dikes, resulting in a dike pole of (225.8°/4.2°). The fact that thick dikes have a present mean orientation more inclined to the north with respect to the thin dikes may indicate that these dikes have undergone a larger amount of tilting. Consequently, this tilting probably occurred during more than one stage.

Thick dikes and granitoids that show the C component of magnetization, exhibit subtle changes, if any, in paleomagnetic inclination (Fig. 13), suggesting that these rocks were remagnetized during a later tectonic event. This hypothesis is in agreement with the homogeneity of paleomagnetic directions of normal polarity in all these rocks (Fig. 13, Table 5) and the higher values of magnetic susceptibility in thick dikes and granitoids with respect to the thin dikes. The characteristic directions of thick dikes and granitoids are roughly similar

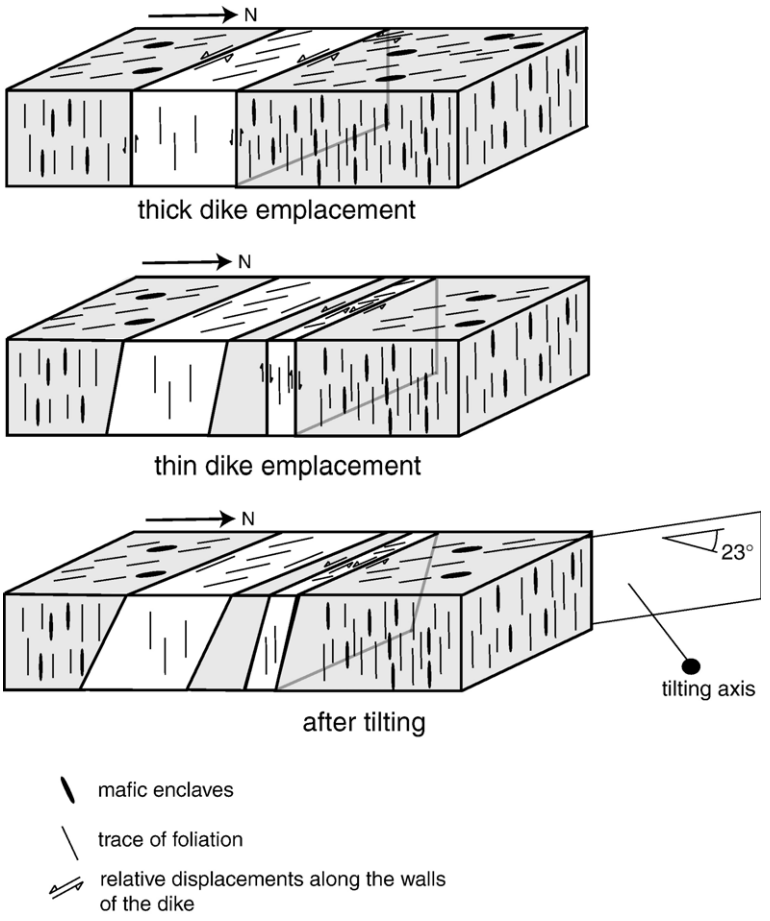

Fig. 14. Schematic representation of emplacement mechanism of the CMDS, with relative shear movements along margins of the intrusions.

to the direction expected for the Early–Mid Cretaceous at this latitude (expected direction of 2.6°/−52.7°). In addition, the exclusive observation of normal polarity magnetization suggests that the rocks were remagnetized during the Cretaceous Long Normal Superchron (118–83 Ma). In fact, the most important post-Jurassic thermo-tectonic event registered in the Coastal Range of central Chile is represented by the rapid exhumation of Paleozoic and Mesozoic units during the Mid-Cretaceous, around 100 Ma, as noted by geological and fission track evidence (Gana and Zentilli, 2000; Arancibia, 2004; Parada et al., 2005). This tectonic event is related to the changes from extensional to compressional conditions in the central Chilean Andean margin.

8.3. Tectonic implications of the CMDS

Taking into account the accumulated thickness of the dikes conforming the CMDS, the emplacement of this swarm represents a minimum of 2.5–4% of crustal dilation.

The Middle Jurassic extension, deduced from our study, can be directly compared with Middle Jurassic extension observed in northern Chile, in terms of the kinematics of crustal extension. An important source of information about the Jurassic tectonic evolution is the Atacama Fault System (AFS), that was most active between 190 and 110 Ma (e.g. Scheuber and Andriessen, 1990; Brown et al., 1993; Grocott and Taylor, 2002). This large broadly N–S trending structural system extends for about 1000 km along the forearc of the central Andes, between 21° and 30° S. The study of this structure and related rocks emplaced along it, indicates that during the Middle Jurassic, there was extension orthogonal to the margin related to strain partitioning caused by oblique, NW–SE, slow convergence between the Aluk and South American plates (Scheuber and Andriessen, 1990). This extension is also recorded by sinistral displacements along the AFS. On the other hand, at 27° S, Taylor and Randall (2000) studied a group of mafic dike swarms of Late Triassic, Middle Jurassic

and Early Cretaceous age that are intruded into associated plutonic complexes. The Middle Jurassic dikes have whole rock $^{40}Ar/^{39}Ar$ dates between 155 and 153 Ma (Dallmeyer et al., 1996), and are intruded into the Las Animas plutonic complex (159–153 Ma, Dallmeyer et al., 1996). Structural analyses of these dikes yield a near horizontal net extension direction with an azimuth of 232°, discarding effects of regional tilting and giving an extension direction that is consistent with oblique subduction during the Jurassic. Middle –Late Jurassic mafic dikes (155–140 Ma) has been reported south of Antofagasta (23° S) by Scheuber and Gonzalez (1999). These consist of an early generation of NE-trending dikes intruded by NW-trending dikes, suggesting that both dike groups intruded during two episodes of contrasting extensional direction, being both oblique to the Jurassic arc. These strong changes were probably controlled by successive seismic decoupling and coupling of the plates along the subduction zone. In contrast, Yañez et al. (1998) presented a model of compressional deformation and SE directed crustal viscous flow associated with oblique convergence for central Chile (33°–34° S), to explain the development of the Melipilla Anomaly and associated currently exposed fault zones. At first sight, the current results about crustal extension derived from the CMDS appear to be inconsistent with the models of Yañez et al. (1998) and with the extension directions obtained for the Jurassic in northern Chile. Geological patterns in Mesozoic and older basement rocks point to a major change in tectonic features in this area of central Chile with respect to those observed in northern Chile. These features of central Chile include: a) absence of large, N–S trending fault systems such as the AFS; b) dominance of NW-trending structures in this area, observed in the CMDS and Jurassic plutons; c) basement of the area, constituted by Late Paleozoic and Late Triassic granitoids with strong ductile deformation, including metamorphic rocks of migmatitic grade, that are in large part absent in the Paleozoic batholith in other latitudes; d) a major change in the orientation axis of the Jurassic batholith, from N–S to the north to nearly NW–SE at 33°. All these geological features suggest that the tectonic evolution of the margin at 33° S evolved in a different way with respect to the Mesozoic evolution described in northern Chile, probably marking a segmentation of the Jurassic margin. The tectonic mechanisms associated to the extensional processes can show local differences controlled by several factors such as the effect of basement inherited structures. However, extension direction deduced from NE-trending dikes in the Antofagasta area (Scheuber and Gonzalez, 1999) are not fairly different from the extension direction deduced for the CMDS and we cannot discard that changes in the interactions between both plates (decoupling and coupling) also plays an important role in the development of the successive generations of dikes in the CMDS.

9. Concluding remarks

The CMDS is composed of two groups of mafic dikes: an early group of thick dikes and a late group of thin dikes that crosscut the thick dikes. The new $^{40}Ar/^{39}Ar$ results on both groups of intrusions demonstrate that the CMDS was emplaced during the formation of the Middle Jurassic arc of central Chile. The high temperature (solid-state) to magmatic fabrics in the mafic dikes, together with the asymmetrical fabrics indicate that the emplacement of the CMDS was syntectonic, associated with sinistral displacement along the host fractures of the magmas. These results suggest that the regional stress field was a dominant factor during the development of the CMDS fabrics. The paleomagnetic studies of thick dikes and granitoid country rocks show characteristic directions of normal polarity that are similar to the paleomagnetic directions expected for the Early Cretaceous. This suggests that these rocks of high susceptibility were remagnetized during the Cretaceous Long Normal Superchron (118–83 Ma), probably associated with the exhumation of deep-seated Paleozoic and Mesozoic coastal rocks around 100 Ma. On the other hand, paleomagnetic directions obtained in thin dikes are interpreted as primary, and indicate that the whole area underwent NNW-directed block tilting during the Mesozoic extension. The NNW sense of tilting deduced from these paleomagnetic results is coincident with the direction of extension deduced from the internal fabric of the dikes, where magnetic lineations are oriented in a NNW–SSE direction. These features allow us to conclude that the evolution of the CMDS during the Jurassic was associated with an extensional event in NNW–SSE direction and that dike emplacement was controlled by NW-trending structures. This kinematic framework for the Mesozoic extensional tectonics is different from the results obtained by other investigators of Jurassic features of northern Chile, pointing to major heterogeneities in the overriding plate during this extensional period. These heterogeneities can be produced by differences in the crustal structure in the overriding plate or by other regional controls in the extensional mechanisms.

Acknowledgments

This research was funded by Fondecyt Project N° 1031000 (leader DM). We thank Natalia Astudillo for

her assistance on a one day field trip, Juan Vargas for his valuable assistance with mineral separation and Mauricio Belmar for helping us with the microprobe analyses at the Departamento de Geología, Universidad de Chile. Microprobe analyses at Zelmi, TU-Berlin, were carried out by the first author with financing of TU-Berlin and a DAAD scholarship, under guidance of Prof. Dr. Gerhard Franz (TU-Berlin) and with the valuable assistance of Francois Galbert and Irene Preuss. The first author carried out his PhD studies with a financial grant from a MECESUP scholarship. The authors would also like to thank Sven Nielsen and Paulina Vásquez for valuable comments on an earlier version of the manuscript and Prof. Jacobous Le Roux and Karen Grove for corrections on the English version of the text. We also thank the editor Mark Sandiford, José Cembrano and an anonymous reviewer for their constructive reviews that improved the manuscript.

References

Aguirre, L., Féraud, G., Morata, D., Vergara, M., Robinson, D., 1999. Time interval between volcanism and burial metamorphism and rate of basin subsidence in a Cretaceous Andean extensional setting. Tectonophysics 313, 433–447.

Anderson, E.M., 1951. The Dynamics of Faulting. Oliver and Boyd, Edinburgh.

Arancibia, G., 2004. Mid-Cretaceous crustal shortening: evidence from a regional-scale ductile shear zone in the Coastal Range of central Chile (32° S). Journal of South American Earth Sciences 17, 209–226.

Arancibia, G., Matthews, S., Pérez de Arce, C., 2006. K–Ar and $^{40}Ar/^{39}Ar$ geochronology of supergene processes in Atacama Desert, northern Chile: tectonic and climatic relations. Journal of the Geological Society of London 163 (1), 107–118.

Arce, M. 2002. Condiciones de formación y naturaleza de las estructuras del complejo plutónico Santo Domingo, V Región: evidencias de terreno y de fábricas magnéticas. Unpublished Thesis. Universidad de Chile.

Arriagada, C., Roperch, P., Mpodozis, C., Dupont-Nivet, G., Cobbold, P., Chauvin, A., Cortés, J., 2003. Paleogene clockwise tectonic rotations in the forearc of central Andes, Antofagasta region, northern Chile. Journal of Geophysical Research 108, 1–22.

Beck Jr., M., Drake, R., Butler, R., 1986. Paleomagnetism of Cretaceous volcanic rocks from central Chile and implications for the tectonics of the Andes. Geology 14, 132–136.

Beck Jr., M., Burmester, R., García, A., Rivano, S., 1990. Paleomagnetic results from the Cretaceous rocks in the Llaillay — San Felipe–Putaendo region: implications for block rotations in the Andean forearc. Revista Geológica de Chile 17, 115–130.

Besse, J., Courtillot, V., 2002. Apparent and true polar wander and the geometry of the geomagnetic field in the last 200 million years. Journal of Geophysical Research 107, 2300.

Blumenfeld, P., Bouchez, J.L., 1988. Shear criteria in granite and migmatite deformed in the magmatic and solid states. Journal of Structural Geology 10 (4), 361–372.

Bouchez, J-L., Delas, C., Gleizes, G., Nédélec, A., Cuney, M., 1992. Submagmatic microfractures in granites. Geology 20, 35–38.

Brown, M., Díaz, F., Grocott, J., 1993. Displacement history of the Atacama Fault System, 25°00′ S–27°00′ S, northern Chile. Geological Society of America Bulletin 105, 1165–1174.

Callot, J.-P., Geoffroy, L., 2004. Magma flow directions in the East Greenland dyke swarm inferred from studies of anisotropy of magnetic susceptibility: magmatic growth of a volcanic margin. Geophysical Journal International 159, 816–830.

Cembrano, J., Gonzalez, G., Arancibia, G., Ahumada, I., Olivares, V., Herrera, V., 2005. Fault zone development and strain partitioning in an extensional strike-slip duplex: a case study from the Mesozoic Atacama fault system, Northern Chile. Tectonophysics 400, 105–125.

Cordani, U., Munizaga, F., Hervé, F., Hervé, M., 1976. Edades provenientes del basamento cristalino de la Cordillera de la Costa de las provincias de Valparaiso y Santiago, Chile. 1° Congreso Geológico Chileno, Departamento de Geología, Universidad de Chile, Santiago, Chile, pp. 213–221.

Correa-Gomes, L.C., Souza Filho, C.R., Martins, C.J.F.N., Oliveira, E.P., 2001. Development of symmetrical and asymmetrical fabrics in sheet-like igneous bodies: the role of magma flow and wall-rock displacements in theoretical and natural cases. Journal of Structural Geology 23, 1415–1428.

Corvalán, J., Munizaga, F. 1972. Edades radiométricas de rocas intrusivas y metamórficas de la Hoja Valparaíso — San Antonio. Instituto de Investigaciones Geológicas, Boletín N28°, 28p. Santiago.

Dallmeyer, R.D., Brown, M., Grocott, J., Taylor, G.K., Treloar, P., 1996. Mesozoic magmatic and tectonic events within the Andean plate boundary zone, 26°–27°30′ S, North Chile: constrains from $^{40}Ar/^{39}Ar$ mineral ages. Journal of Geology 104, 19–40.

Delaney, P.T., Pollard, D.D., Ziony, J., Mckee, E.H., 1986. Field relations between dikes and joints: emplacement processes and paleostress analysis. Journal of Geophysical Research 91, 4920–4938.

Ernst, R.E., Grosfils, E.B., Mège, D., 2001. Giant dyke swarms: Earth, Venus and Mars. Annual Review of Earth and Planetary Science 29, 489–534.

Féménias, O., Diot, H., Berza, T., Gauffriau, A., Demaiffe, D., 2004. Asymmetrical to symmetrical magnetic fabric of dikes: paleo-flow orientations and paleo-stresses recorded on feeder-bodies from the Motru Dike Swarm (Romania). Journal of Structural Geology 26, 1401–1418.

Ferré, E., Teyssier, C., Jackson, M., Thill, J., Rainey, E., 2003. Magnetic susceptibility anisotropy: a new petrofabric tool in migmatites. Journal of Geophysical Research 108, B2,doi: 10.1029/2002JB001790.

Gana, P., Tosdal, R., 1996. Geocronología U–Pb y K–Ar en intrusivos del Paleozoico y Mesozoico de la Cordillera de la Costa, Región de Valparaíso, Chile. Revista Geológica de Chile 23, 151–164.

Gana, P., Zentilli, M., 2000. Historia termal y exhumación de intrusivos de la Cordillera de La Costa de Chile Central. 9° Congreso Geológico Chileno. Servicio Nacional de Geología y Minería, Puerto Varas, Chile, vol. 1, pp. 664–667.

Gana, P., Wall, R., Gutiérrez, A., 1996. Mapa geológico del área de Valparaíso-Curacaví. Servicio Nacional de Geología y Minería. Mapas Geológicos, N°1, escala 1: 100.000. Santiago.

Geoffroy, L., Callot, J.P., Aubourg, C., Moreira, M., 2002. Divergence between magnetic and plagioclases linear fabric in dykes: a new approach to defining the flow vector using magnetic foliation. Terra Nova 14, 183–190.

Glazner, A., Bartley, J., Carl, B., 1999. Oblique opening and noncoaxial emplacement of the Jurassic independence dike swarm, California. Journal of Structural Geology 21, 1275–1283.

Godoy, E., Loske, W., 1988. Tectonismo sinplutónico de dioritas jurásicas al sur de Valparaíso: datos U–Pb sobre la Fase Quintay. Revista Geológica de Chile 15, 119–127.

Grocott, J., Taylor, G.K., 2002. Deformation partitioning, magmatic arc fault systems and the emplacement of granitic complexes in the Coastal Cordillera, north Chilean Andes (25–27° S). Journal of Geological Society of London 159, 425–442.

Hervé, F., Munizaga, F., Parada, M.A., Brook, M., Pankhurst, R., Snelling, N., Drake, R., 1988. Granitoids of the Coast Range of central Chile: geochronology and geologic setting. Journal of South American Earth Sciences 1, 185–194.

Holland, T., Blundy, J., 1994. Non-ideal interactions in calcic amphiboles and their bearing on amphibole–plagioclase thermometry. Contributions to Mineralogy and Petrology 116, 433–444.

Hutton, D., 1992. Granite sheeted complexes: evidence for the dyking ascent mechanism. Transactions of the Royal Society of Edinburgh. Earth Sciences 83, 377–382.

Irving, E., Baker, J., Wynne, P.J., Hamilton, T.S., Wingate, M.T.D., 2000. Evolution of the Queen Charlotte Basin; further paleomagnetic evidence of Tertiary extension and tilting. Tectonophysics 326, 1–22.

Irwin, J., Sharp, W., Spangler, R., Drake, R., 1987. Some paleomagnetic constraints in the tectonic evolution of the coastal cordillera of central Chile. Journal of Geophysical Research 92, 3603–3614.

Irwin, J., García, C., Hervé, F., Brook, M., 1988. Geology of a part of a long-lived dynamic plate margin: the Coastal Cordillera of north-central Chile, latitude 30°51′–31° S. Canadian Journal of Earth Sciences 25, 603–624.

Isacks, B.L., 1988. Uplift of the central Andean Plateau and bending of the Bolivian orocline. Journal of Geophysical Research 93, 3211–3231.

Johnson, A.M., Pollard, D.D., 1973. Mechanisms of growth of some laccolithic intrusions in the Henry Mountains, Utah. Field observations, Gilbert's model, physical properties and flow of the magma. Tectonophysics 18, 261–309.

Karson, J., Hurst, S., Lonsdale, P., 1992. Tectonic rotation of dykes in fast-spread oceanic crust exposed near Hess Deep. Geology 20, 685–688.

Knight, D., Walker, M., 1988. Magma flow direction in dykes of Koolau Complex, Oahu, determined from magnetic fabric studies. Journal of Geophysical Research B5, 4301–4319.

Levi, B., 1973. Eastern shift of Mesozoic and Early Tertiary volcanic centers in the Coast Range of central Chile. Geological Society of America Bulletin 84, 3901–3910.

Mège, D., Korme, T., 2004. Dyke swarm emplacement in the Ethiopian Large Igneous Province: not only a matter of stress. Journal of Volcanology and Geothermal Research 132, 283–310.

Morata, D., Aguirre, L., 2003. Extensional Lower Cretaceous volcanism in the Coastal Range (29°20′–30° S), Chile: geochemistry and petrogenesis. Journal of South American Earth Sciences 16, 459–476.

Morata, D., Aguirre, L., Féraud, G., Fuentes, F., Parada, M.A., Vergara, M., 2001. The Lower Cretaceous volcanism in the Coastal Range of central Chile: geochronology and isotopic geochemistry, III South American Symposium on Isotope Geology. Sociedad Geológica de Chile, Pucón, Chile, pp. 321–324.

Mpodozis, C., Ramos, V., 1989. The Andes of Chile and Argentine. Circum Pacific Council for Energy and Mineral Resources. Earth Science Series 11, 59–88.

Muñoz Cristi, J., 1964. Estudios petrográficos y petrológicos sobre el Batolito de la Costa de las provincias de Santiago y Valparaíso. Publicación 25, Universidad de Chile. 94 pp.

Parada, M.A., Levi, B., Nystrom, J., 1991. Geochemistry of the Triassic to Jurassic plutonism of central Chile (30° to 33° S); petrogenetic implications and a tectonic discussion. Geological Society of America Special Paper 265, 99–112.

Parada, M.A., Nystrom, J., Levi, B., 1999. Multiple sources for the Coastal batholith of central Chile (31–34° S): geochemical and Sr–Nd isotopic evidence and tectonic implications. Lithos 46, 505–521.

Parada, M.A., Féraud, G., Fuentes, F., Aguirre, L., Morata, D., Larrondo, P., 2005. Ages and cooling history of the Early Cretaceous Caleu pluton: testimony of a switch from a rifted to a compressional continental margin in central Chile. Journal of the Geological Society of London 162, 273–287.

Paterson, S., Vernon, R., Tobish, J., 1989. A review of criteria for the identification of magmatic and tectonic foliations in granitoids. Journal of Structural Geology 11, 349–363.

Scarrow, J., Leat, P., Wareham, C., Millar, I., 1998. Geochemistry of mafic dykes in the Antarctic Peninsula continental-margin batholith: a record of arc evolution. Contributions to Mineralogy and Petrology 131, 289–305.

Scheuber, E., Andriessen, P.A.M., 1990. The kinematics and geodynamics significance of the Atacama Fault Zone, Northern Chile. Journal of Structural Geology 12, 243–257.

Scheuber, E., Gonzalez, G., 1999. Tectonics of the Jurassic–Early Cretaceous magmatic arc of the north Chilean Coastal Cordillera (22°–26° S): a history of crustal deformation along a convergent plate boundary. Tectonics 18 (5), 895–910.

Simpson, C., 1985. Deformation of granitoid rocks across the brittle–ductile transition. Journal of Structural Geology 7, 503–511.

Tauxe, L., Gee, J.S., Staudigel, H., 1998. Flow directions in dikes from anisotropy of magnetic susceptibility data: the bootstrap way. Journal of Geophysical Research 103, 17775–17790.

Taylor, G.K., Randall, D., 2000. Structural analysis of dyke emplacement directions as an aid to paleomagnetic studies: an example from northern Chile. Geophysical Journal International 141, 253–258.

Vergara, M., Levi, B., Nystrom, J., Cancino, A., 1995. Jurassic and Early Cretaceous island arc volcanism, extension and subsidence in the Coast Range of central Chile. Geological Society of America Bulletin 107, 1427–1440.

Yañez, G., Gana, P., Fernández, R., 1998. Origen y significado geológico de la Anomalía Melipilla, Chile central. Revista Geológica de Chile 25 (2), 175–198.